Study of the Fourier phase shift method (FPS) for asymmetrical spots — comparison with a centroid method —

Paul ROYO [1,2]

1: Student of Département de physique de l'EPFL
Ecole Polytechnique Fédérale de Lausanne,Ecublens, CH - 1015 Lausanne
2: Summer trainee in the Applied Optics Group
Blackett Laboratory, Imperial College, London SW7 2BZ, United Kingdom

1 Introduction

The aim of this work is to localize with a high accuracy (subpixel accuracy) the position of a spot in a pixel array. The study of this type of problem is essential for the realization of a wavefront analyzer as the Shack-Hartmann sensor.

In the first section of this report we will recall the fundamentals of the Shack-Hartmann sensor and explain the problem to be solved. In the second part, we will present different methods found in the literature to analyse a wave front by measuring the spots of the Shack-Hartmann sensor and try to classify them. Then a specific method, the Fourier phase shift method, will be introduced and in the fourth and last section we will present the results of our simulations.

2 The Shack-Hartmann sensor - review

2.1 Generalities

The principle of this system is given in the figure 1. The idea is to analyse the wavefront in dividing it spatially by a lenslet array. Considering that each of the pieces is a plane wave, it is possible to analyse the whole wave front by analysing each of the individual waves. As it is indeed explained in reference [30] , if a wavefront can be spatially divided, and individual wavefront slopes (or tilts) can be determined, then the entire wavefront across an aperture can be determined. So the problem comes down to determining the tilt of a single plane wave. Differents methods exist, and the ones that interest us are based on measure of spot displacements (other methods that rely on interferometry for example, have also been developed but are not considered in this work).

2.2 Measurement of the local wavefront slope

It is possible to show [30] that wavefront tilt displaces a focused image (without changing the focus) in the direction of the tilt and at a distance proportional to amount of tilt (see Fig. 2). Theoretically, focusing a plane wave by a lens gives a point in the focal plane (see Fig. 3). Nevertheless propagation of the plane wave through a circular aperture and the lens, will result in an Airy disk spot, due to diffraction [25] (see Fig. 4). It is possible to introduce the centroid of the intensity distribution to characterize the shape of the spot. The interesting thing is that the tilt of the plane wave will shift the position of the intensity centroid in the focal plane, and that other aberrations (tilt can be considered as a geometric aberration) change the shape of the pattern and position of the maximum, but don't shift the centroid. Figure 5 summarizes these points.

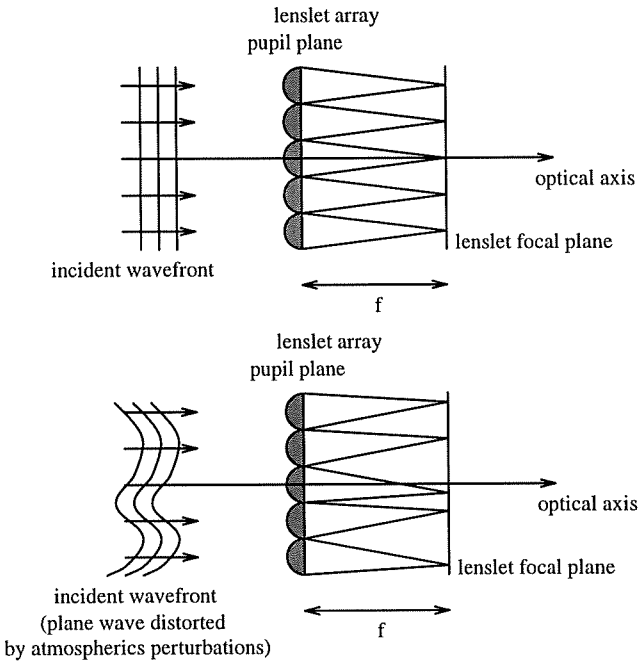

Figure 1: Principle of the Shack-Hartmann sensor. The displacements of the spots are proportional to the local wavefront slopes

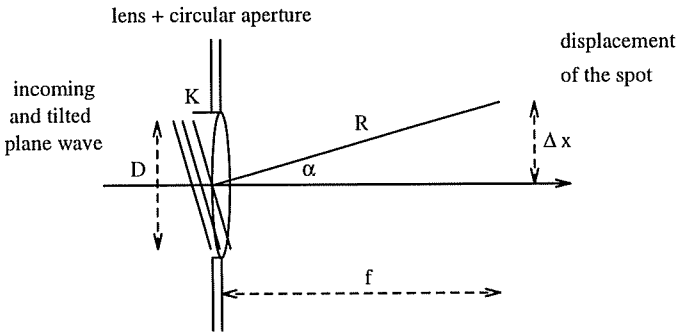

Figure 2: For a tilt of K, the spot will move of $\Delta x = \frac{2RK}{D} = \alpha f$

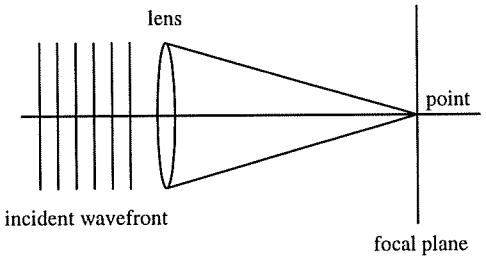

Figure 3: Ideal focusing

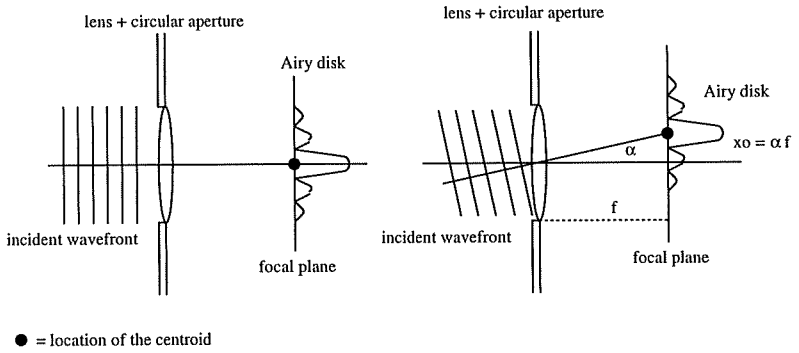

Figure 4: Displacement of the Airy disk (spot) when no aberrations

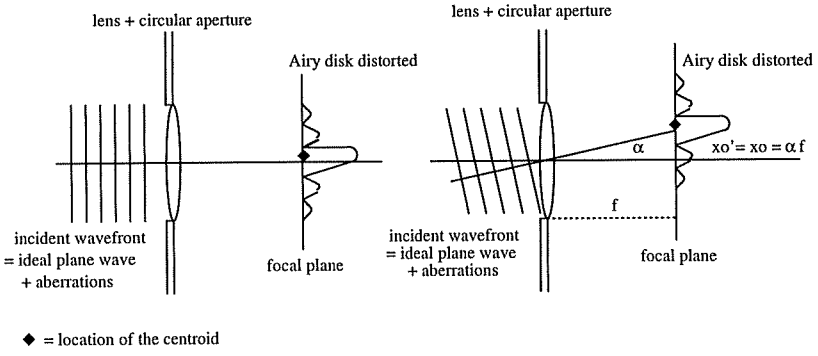

Figure 5: Displacement of the Airy disk (spot) when aberrations

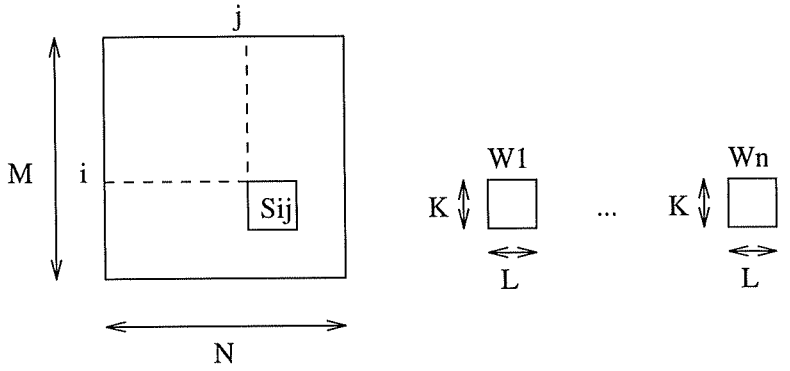

Figure 6: Search area S and subimages W_i

3 Summary of existing methods used to locate a spot displacement

The aim of this section is to present differents methods to locate a spot in an array of pixels. Theses methods can be classify in two categories: the methods where the accuracy can not be better than one pixel and the others where the accuracy can be of subpixel order.

3.1 Pixel accuracy methods

3.1.1 Multiple images registration algorithms

Two different problems can be distinguished. We can first consider that we have one array of pixels and several subimages in it. In the case of the Shack-Hartmann, we could have to find n spots (subimages) in one array of pixels. This type of problem has been studied in reference [22]. In figure 6 we show the search arrea S (which is an M*N array of digital pictures elements) and n subwindows $W_1, ..., W_n$ of size K*L. Each pixel may assume one of G grey levels.

The problem is to recognize each K*L subimage in the search area S; each will be uniquely identified by its upper left corner's coordinates. For exemple S_ij denotes the K*L subimage of S whose upper left corner is (i, j). Boland, Ranganath and Malcom [22] evaluate the computation time of three methods.

First method is the correlation method. Elements of normalized correlation function $R_k^2(i, j)$ of search area S and window W_k are calculated. It is simple to find the coordinates (i_k^*, j_k^*) that maximize $R_k^2(i, j)$; they correspond to the location of the subimage k.

Second method is the sequential similarity detection algorithm (SSDA). This method computes a normalized error between each W_k and each S_ij. A criterion allows to find (i_k^*, j_k^*), the coordinates of subimage k.

Third method is the method of moments. The idea is to calculate the moments of the subimage W_k, to calculate the moments of all the subimages of S, and to register W_k within S in satisfying a given criterion.

The conclusion of this work is that for single image registration problems, the moments method requires more computation time than the two others methods. Nevertheless, for the multiple image registration problem, the moments method becomes computationally more efficient as the number of windows increases. It is also shown that the moments method requires less computation time if implemented in software and less hardware for real time implementation when number of windows is large. The main drawback of this method is that it is not a subpixel accuracy method.

3.1.2 Zero order method

From an other point of view, we can try to locate the subimage by one particular point (the maximum spot for instance), rather than detecting the whole sub-image. This approach is systematically used

in our domain of interest (astronomy and especially Shack-Hartmann sensors) and is refered as image centroiding. The first basic idea is simply to find the center of the disk (we want to locate a theoretically Airy disk in an array of pixels) by selecting the target pixel with the highest output. It is clear that the smaller is the pixel and the better is the resolution. In fact if the pixels are too small, they will not collect enough energy to provide a convenient SNR. Economical reasons (like cost of large array of tiny pixels could also be taken into account). This is the reason why most of the techniques studied in image centroiding are subpixel accuracy techniques: the problem is to locate very precisely the centroid of a spot in an array with a small number of pixels (typically : $8 * 8$ pixels in [6], $24 * 24$ pixels in [13], or $32 * 32$ [10] and $16 * 16$ in Imperial College system).

3.2 Subpixel accuracy methods

3.2.1 Method of moments

It is possible to show that moments of a function completely and uniquely describe that function [18]. For example, if $i(x, y)$ is the intensity distribution of the recorded image, and $o(x, y)$ the intensity of the source, Restaino [23] says that $o(x, y)$ can be expressed in a series :

$$i(x,y) = \sum_{m=0}^{\infty}\sum_{n=0}^{\infty} \frac{a_{mn}}{m!n!} \frac{\partial^{m+n} o(x,y)}{\partial x^m \partial y^n} \tag{1}$$

where:

$$a_{mn} = \int_{-\infty}^{\infty}\int_{-\infty}^{\infty} h(\xi,\eta)\xi^m\eta^n d\xi d\eta \tag{2}$$

are the moments of the PSF, $h(u, v)$. The problem studied in this work (and presented at the beginning of this report), can be understood as a particular case of the series expansion presented above (where $o(x, y)$ describes a plane wave). In practice only moments up to second order are calculated, and to locate the position of the spot, only the first order moment (or centroid) is usefull. The calculation of second order moment is often performed to study the accuracy of the method under noise hypothesis [7] [14] [15].

3.2.2 Centroid method

This is the more used and well-known method. It can be found (in [24] for example) that the centroid $< x >$ of the function $f(x)$ is defined by:

$$< x >= \frac{\int_{-\infty}^{\infty} x f(x) dx}{\int_{-\infty}^{\infty} f(x) dx} = \frac{-\dot{F}(0)}{2\pi i F(0)} \tag{3}$$

with $F(u)$ the Fourier transform of f(x). This coefficient tells us where a function $f(x)$ is mainly concentrated. In statics, $< x >$ is the abscissa of the center of gravity of a rod whose mass density is $f(x)$. So this is the proper coefficient to determine the position of a spot. The above formula is easy to generalize in two dimensions [1]:

$$< x >= \frac{\int_{-\infty}^{\infty}\int_{-\infty}^{\infty} x f(x,y) dx dy}{\int_{-\infty}^{\infty}\int_{-\infty}^{\infty} f(x,y) dx dy} = \frac{-F'_u(0,0)}{2\pi i F(0,0)} \tag{4}$$

$$< y >= \frac{\int_{-\infty}^{\infty}\int_{-\infty}^{\infty} y f(x,y) dx dy}{\int_{-\infty}^{\infty}\int_{-\infty}^{\infty} f(x,y) dx dy} = \frac{-F'_v(0,0)}{2\pi i F(0,0)} \tag{5}$$

with $F(u, v)$ the Fourier transform of f(x,y).

As we are interested in signals provided by a sensor array (CCD most of the time), it is necessary to use the discrete formula below [10]:

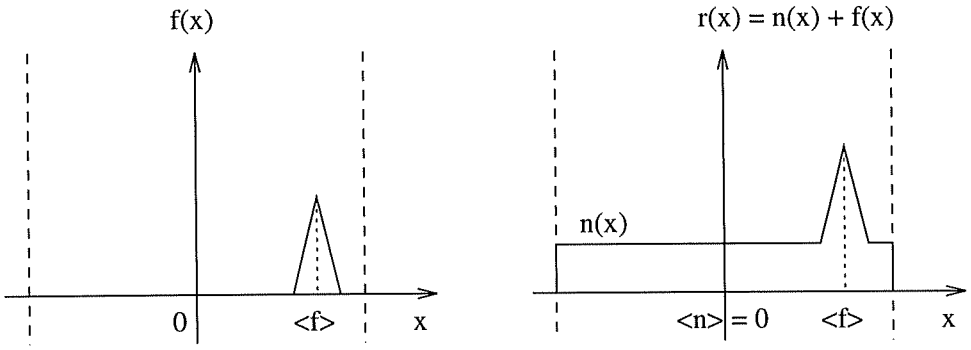

Figure 7: Signal without offset (left): the centroid is in $< f >$; Signal with offset (rigth): the centroid is between $< n >= 0$ and $< f >$

$$< x >= \frac{\sum_k \sum_l k f_{k,l}}{\sum_k \sum_l f_{k,l}} \tag{6}$$

$$< y >= \frac{\sum_k \sum_l l f_{k,l}}{\sum_k \sum_l f_{k,l}} \tag{7}$$

with $f_{k,l} = f(kT, lT)$ and $1/T$ the spatial sample frequency. This method suffers from an important drawback: it is very sensitive to DC-offset and low-frequency noise. This last point is easy to understand, since $< x >$ and $< y >$ can be expressed with the Fourier transfrom of $f(x, y)$ at the frequency $u = v = 0$ (DC frequency). The former problem has been studied in reference [13] and we can explain easily what happens. Suppose we have a perfect signal $f(x)$, on which an offset signal $n(x)$ is added, as shown in figure 7

Then the centroid of $r(x) = n(x) + f(x)$ is given by the expression above:

$$< r >= \frac{\int_{-\infty}^{\infty} x f(x)dx + \int_{-\infty}^{\infty} x n(x)dx}{\int_{-\infty}^{\infty} r(x)dx} = \frac{\int_{-\infty}^{\infty} f(x)dx}{\int_{-\infty}^{\infty} r(x)dx} . < f >= \frac{1}{1 + \frac{\int_{-\infty}^{\infty} n(x)dx}{\int_{-\infty}^{\infty} f(x)dx}} . < f > \tag{8}$$

So, if $n(x)$ becomes important, the centroid $< r >$ of $r(x)$ will get away from the real centroid $< f >$ of $f(x)$. The use of a threshold can help us to get rid of this problem.

3.2.3 Treatment of noisy spots with centroid method

Different analysis of errors have been performed by many authors and two sources of errors are usually considered: first, systematic errors due to the nature of the algorithm, and secondly, errors due to noise.

Alexander [1] showed that if $f(x)$ is the continuous profile and $g(x)$ the corresponding samples profile, a systematic error will be present if the centroid of $g(x)$ is not equal to the centroid of $f(x)$; it is the case if the maximum spatial frequency of the image incident on the sensor is more than the sampling frequency. Fillard [9] concludes that no gate shape and width (pixel sensitivity profile) effects are to be expected in the evaluation of the centroid. A study of the effect of deadspace between detectors and size of the blur spot has been made in ref [4] by Cox.

Concerning errors due to noise, a lot of studies have been made on the effect of noise on centroidind error ([3] [6] [7] [8] [14] [15] [20]), but it's difficult to extract general results of practical interest. Most of the time, two types of noise are considered: the background and the detector noises (both Poisson-distributed), and the shot noise. We can nevertheless retain that reducing the subwindow (the size of sensor array) can help to reduce the centroiding errors caused by the readout noise. But doing this, the dynamic range of image spot will be reduced. So a trade-off must be made between the readout noise and the subwindow size, pixel size and image spot size [3]. The reference [20] gives an interesting result

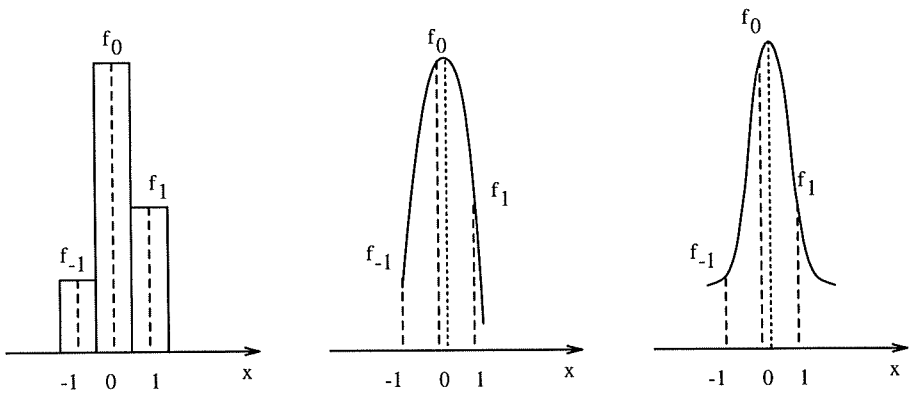

Figure 8: Sampled signal (left), parabolic interpolation (middle) and Gaussian interpolation (rigth)

concerning the pixel-to-image spot size [3].In this study the object's image spot at the CCD is assumed to have a Gaussian intensity profile. The CCD noise is modeled as Poisson-distributed noise, generated by both the image spot and the detector dark current. With these hypotheses, it is demonstrated that there is a pixel-to-image spot size ratio that minimizes the position-estimation errors. For 2D spots, a ratio between 1.5 and 2.5 is found.

3.2.4 Method of cross-correlation

This method is presented by Tyler, Rousset, Restaino and Loos in the reference [19]. In fact it is a modified centroid-method. The aim of this study was to obtain an algorithm to get "a subaperture slope estimator in a low ligth-level adaptive optics scheme for a two-telescope interferometer". We can first recall the definition of the cross-correlation between two functions f and g:

$$C(f,g,r) = \int f(\rho - r)g^*\rho d^2\rho \tag{9}$$

This coefficient can be seen as a distribution of the degree to which f and g are spatially similar at a particular r. It can be easily shown that $\mathcal{F}[C(f,g,r)] = \mathcal{F}(f).\mathcal{F}^*(g)$ In the method of cross-correlation, f is the signal measured, and g is a "template" signal. In the article f was the fringe pattern and g was a 2d sinc function. In the case of the Shack-Hartmann system, f could be the spot signal, and the template g could be an Airy function. The idea of the method is to calculate the centroid of the cross-correlation, but after having found the peak of the cross-correlation and set to zero all the pixels beyond a small radius. As a matter of fact, this last point is crucial, since it can be shown that calculating the centroid of the full cross-correlation function is no improvement over calculating the centroid of the original noisy distribution. The conclusion of the work was that this technique reduces measurement error by significant amount in the presence of additive (CCD) noise, and that for Poisson (shot) noise, the error is reduced to a lesser degree.

3.2.5 Methods of interpolation

An other important class of methods is interpolation methods. Suppose that we have the sampled signal as in figure 8

The idea of these methods is to interpolate a given number of points in the measured signal and to find the maximum of the interpolation curve. Efficients algorithms exist to find an extremum in a function without having to evaluate the function too often (method of bissection for exemple [17]).

The simplest method is the least-squares fit of a parabola to the data points. In the reference [11], three and five points had been used for the interpolation method, but it is shown that the centroid method is to be prefered on interpolation methods (more accurate). An other comparison between centroid method and interpolations methods [4] gives the same conclusion.

According to Seitz [17], because of the central limit theorem, the measured spot should be Gaussian and a Gaussian interpolation could be the proper way of finding the maximum of the spot. In the reference [20] and [11] the authors assume that the spot is a Gaussian shape instead of an Airy disk because of atmosphere turbulence [20] and because of optical aberrations or wide spectral band [11].Moreover a Gaussian profile is an excellent approximation to an Airy profile in its central region. Unfortunately, no usefull conclusions are available on the accuracy with this method [1]

To conclude, the main drawback of interpolation methods comes from the limited number of samples involved, which makes the method very sensitive to perturbations.

4 The Fourier phase shift method (FPS method)

4.1 Principle of this method

This method has been proposed by Fillard [9] [10] and relies on the study of the Fourier transform phase of the signal [2]. In his article Fillard assumes that the signal $f(x)$ (the presentation of the method will be done with a one dimensional signal, the generalization for two dimensional signals is straightforward) is real and symmetrical. If $f(x)$ is even (centred at origin) then its Fourier transform $F(s) = \mathcal{F}[f(x)]$ will have a phase equal to zero over all the frequency domain. Suppose now that $f(x)$ has been shifted a distance x_o from origin. We call $g(x)$ this function, which is given by $g(x) = f(x - x_o)$. Using basic Fourier transform properties [3], we have $G(s) = F(s)e^{-2\pi s x_o i}$. We will use the notation $F(s) = |F(s)|e^{iArg[F(s)]} = |F(s)|e^{i\varphi(s)}$ where $|F(s)|$ is the modulus of $F(s)$, and $\varphi(s) = Arg[F(s)]$ is phase. Therefore $Arg[G(s)] = Arg[F(s)] - 2\pi s x_o = -2\pi s x_o$. To summarize, if we are able to calculate the Fourier transform phase of the spot displaced, then we are able to calculate x_o, and to locate with perfect accuracy the position of the spot. Nevertheless, it is obvious that the "signal" $f(x)$ is in reality the PSF function of an optical system with a diffraction-limited circular aperture under Fraunhoffer paraxial and far-field approximation, subject to different noises. Moreover this signal will be sampled and quantized by the detectors array. In the paper [9], Fillard concludes that FPS method is :

- quite immune to gate shape and width
- quite immune to dc-offset reduction
- quite immune to low-frequency noise
- tolerant to deviations to prerequisite symmetry of the signal

This method can also be used without any previous knowledge or model for the exact shape of the signal, provided that the function would be symmetrical.

In a second paper [10] Fillard and al. present two computer simulations of the analysis of a two-dimensional Airy disk and a comparison between FPS method and the traditional centroid calculation method (CCM). The conclusion of this work is that from the evaluation of the calculation errors on quantized data (8bits) in the reference pixel, the maximum error is 1.5% of a pixel with the CCM and 0.35% with the FPS. In addition the FPS calculation is said to be more accurate and less sensitive to external perturbation such as stray light, optical distorsions and electronic noise.

To conclude this subsection, we can now define the objectives of this work. The problem with this comparison is that Fillard and al. compare FPS method with a very simple CCM method. A high performance CCM method has been implemented at Imperial College and the purpose of this work is to try to compare again FPS method with the Imperial College CCM. In addition, as far as we know, the influence of asymmetry on FPS method has not been really studied by Fillard. This is a very important point, since spots measured by a Shack-Hartmann sensors are all but symmetrical.

[1] Seitz [17] in fact studied the problem of the determination of the exact location of an edge, (black and white transition), which is a problem far from our's

[2] "signal" must be understood as "light intensity of the spot signal"

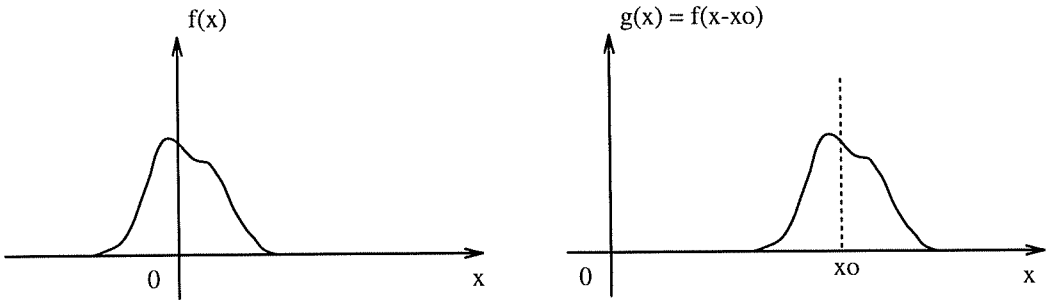

Figure 9: Spot centred $f(x)$ and spot shifted $g(x)$

4.2 Effects of asymmetry on the FPS method

We will work with an asymmetrical and one dimensional signal $f(x)$ supposed to describe one of the spot of the Shack-Hartmann sensor. As shown in the figure 9, $f(x)$ is the spot "centred", that means $f(x)$ describes the spot that would be measured if the plane wave would not have a tilt; 0 could be the middle of the sensor array. We will call $g(x)$ the spot displaced of x_o from the origin 0, because of the plane wave tilt. It is always possible to express a function of any shape $f(x)$ as the sum of an even function $e(x)$ and an odd function $o(x)$:

$$f(x) = e(x) + o(x) \quad e(-x) = e(x) \quad o(-x) = -o(x) \tag{10}$$

where :

$$e(x) = \frac{f(x) + f(-x)}{2} \qquad o(x) = \frac{f(x) - f(-x)}{2} \tag{11}$$

We can define the Fourier transform of $f(x)$ by $F(s) = O(s)+E(s)$ where $O(s) = Re[O(s)]+iIm[O(s)]$ and $E(s) = Re[E(s)] + iIm[E(s)]$, so $F(s) = \{Re[O(s) + Re[I(s)]\} + i\{Im[O(s)] + Im[I(s)]\} = R(s) + iI(s)$ with $R(s)$ and $I(s)$ reals. We can find analytical expression for R(s) and I(s) in [3]:

$$R(s) = 2\int_0^\infty e(x)cos(2\pi xs)dx \tag{12}$$

$$I(s) = -2\int_0^\infty o(x)sin(2\pi xs)dx \tag{13}$$

As shown above, we have $G(s) = F(s)e^{-2\pi s x_o i} = [R(s) + iI(s)].[cos(2\pi s x_o) - isin(2\pi s x_o)]$. The problem to solve is this one: $|G(s)|$ and $Arg[G(s)] = \psi(s)$ can be calculated from $g(x)$ (measured), and we want to determine x_o. For this purpose, we will calculate $a(s) = tan\{Arg[G(s)]\} = tan[\psi(s)]$:

$$a(s) = \frac{Im[G(s)]}{Re[G(s)]} = \frac{I(s)cos(2\pi s x_o) - R(s)sin(2\pi s x_o)}{R(s)cos(2\pi s x_o) + I(s)sin(2\pi s x_o)} \tag{14}$$

As we are interested in knowing x_o, we will take the first derivative of $a(s)$ to try to make appear x_o. After some calculations we find that:

$$\frac{\partial a(s)}{\partial s} = \frac{-2\pi x_o[I^2(s) + R^2(s)] + \dot{I}(s)R(s) - \dot{R}(s)I(s)}{[R(s)cos(2\pi s x_o) + I(s)sin(2\pi s x_o)]^2} \tag{15}$$

It is impossible to obtain x_o from $\frac{\partial a(s)}{\partial s}$, unless we try to evaluate $\frac{\partial a(s)}{\partial s}$ in $s = 0$. From the analytical expressions of $R(s)$ and $I(s)$, we can show easily that :

$$\begin{cases} R(0) \neq 0 \\ \dot{R}(0) = 0 \end{cases} \quad and \quad \begin{cases} I(0) = 0 \\ \dot{I}(0) \neq 0 \end{cases} \tag{16}$$

Consequently, we find that:

$$\frac{\partial a(s)}{\partial s}\Big)_{s=0} = -2\pi x_o + \frac{\dot{I}(0)}{R(0)} \tag{17}$$

Noting that the centroid $< x >$ of the function $f(x)$ is given [24] by:

$$< x >= \frac{\int_{-\infty}^{\infty} x f(x) dx}{\int_{-\infty}^{\infty} f(x) dx} = \frac{-\dot{F}(0)}{2\pi i F(0)} \tag{18}$$

we can simplify the above equation since $F(s) = R(s) + iI(s) \Rightarrow F(0) = R(0)$ and $\dot{F}(0) = i\dot{I}(0)$. Thus $< x >= -\frac{\dot{I}(0)}{2\pi R(0)}$ and it comes finally:

$$\frac{\partial a(s)}{\partial s}\Big)_{s=0} = -2\pi \left[x_o + < x >\right] \tag{19}$$

where x_o is the displacement of the spot, and $< x >$ the centroid **of the spot centred** $f(x)$. We have defined $a(s)$ as $a(s) = tan[\psi(s)]$ with $\psi(s)$ the phase of the Fourier transform of $g(x)$. So $\frac{\partial a(s)}{\partial s} = \frac{\partial \psi(s)}{\partial s} \cdot \frac{1}{cos^2[\psi(s)]}$, and finally:

$$\begin{gathered} \frac{\partial \psi(s)}{\partial s}\Big)_{s=0} = -2\pi \left[x_o + < x >\right] . cos^2[\psi(0)] \\ \psi(s) = Arg\left\{\mathcal{F}[g(x)]\right\} \end{gathered} \tag{20}$$

We can retrieve the result of Fillard (for $f(x)$ symmetrical and even) imposing $o(x) = 0 \ \forall x$.In this case $< x >= 0$ (an even function is always centred at its centroid), so $\psi(s) = -2\pi s x_o$ and $\frac{\partial \psi(s)}{\partial s}\Big)_{s=0} = -2\pi x_o$

To conclude, if we are able to calculate the phase $\psi(s)$ of the Fourier transform of the spot, and if we are able to evaluate the slope of $\psi(s)$ in $s = 0$, then we will be able to determine x_o.

4.3 Verification of the validity of the FPS method with simple (1D) signals

We will test the method on two simple shapes. The Fourier transform will be calculated with 64 samples.

4.3.1 Rectangular signal

We will start with a perfect symmetrical and even signal, the rectangular function. We have chosen five (odd number) non-zeros samples to avoid sampling effects. Figure 10 and 11 shows $f(x), F(s), \psi(s)$, $\frac{\partial \psi(s)}{\partial s}$ and $\frac{\partial^2 \psi(s)}{\partial s^2}$. We see that as expected, $\psi(s)$ is a straight line and $\frac{\partial \psi(s)}{\partial s}$ a flat line. The measurement of the slope of $\psi(s)$ gives $\frac{\partial \psi(s)}{\partial s} = -0.9817$. We can see on the figure that $g(x) = f(x - x_o)$ with $x_o = 10$. As we work with numerical data, the phase will be given by $\psi(s) = \frac{-2\pi s x_o}{NT}$ with s the discrete frequency, x_o the displacement we want to get, N the number of samples (here $N = 64$) and T^{-1} the sampling frequency of $g(x)$ (here $T = 1$ arbitrarely). So we must measure an ideal slope of $\frac{-2\pi.10}{64} = -0.9817477042$ that is what we have measured on the phase calculated by FFT.

4.3.2 Triangular signal

The second signal studied is strongly asymmetrical since it is a triangle signal. The calculation of the phase $\psi(s)$ of the Fourier transform makes appear a curve that seems to be a straight line. The first and second derivatives of $\psi(s)$ have been plotted and we see that around the frequencies origin (in $s = 33$) [3], the first derivative doesn't vary very much. This result confirms us that calculating the slope of the phase at the origin can be made. We have thought at two methods to determine the slope of the phase at the origin.The first idea was to calculate it by means of a linear fit (least mean square for instance). The method is correct if the signal is symmetrical, since the phase must be a straight line. If the signal

[3] In our simulations, we have used a function that fix the DC frequency at the point $\frac{N}{2} + 1$ with N, the number of samples used

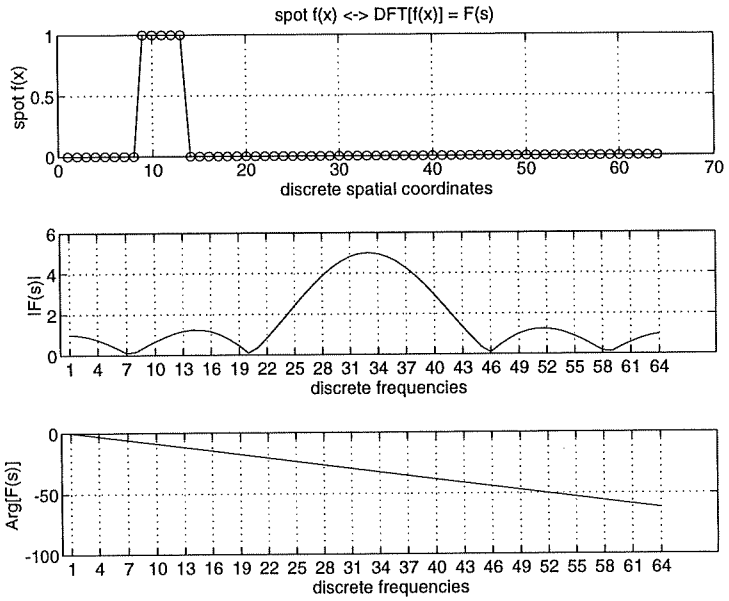

Figure 10: Rectangular signal, modulus of its Fourier transform and phase

is not symmetrical, the more points we will take for the regression, and the worse the evaluation of the slope will be. That is why, we have used formulas for central derivatives given by [29].

Order = 2:

$$\frac{\partial\psi(s)}{\partial s}\Big)_{s=0} \simeq \frac{1}{h}[\psi(1)-\psi(-1)] - \frac{h^2}{6}\psi^{(3)} \tag{21}$$

Order = 4:

$$\frac{\partial\psi(s)}{\partial s}\Big)_{s=0} \simeq \frac{2}{3h}[\psi(1)-\psi(-1)] - \frac{1}{12h}[\psi(2)-\psi(-2)] + \frac{h^4}{30}\psi^{(5)} \tag{22}$$

Order = 6:

$$\frac{\partial\psi(s)}{\partial s}\Big)_{s=0} \simeq \frac{3}{4h}[\psi(1)-\psi(-1)] - \frac{3}{20h}[\psi(2)-\psi(-2)] + \frac{1}{60h}[\psi(3)-\psi(-3)] - \frac{h^6}{140}\psi^{(7)} \tag{23}$$

Order = 8:

$$\frac{\partial\psi(s)}{\partial s}\Big)_{s=0} \simeq \frac{4}{5h}[\psi(1)-\psi(-1)] - \frac{1}{5h}[\psi(2)-\psi(-2)] + \frac{4}{105h}[\psi(3)-\psi(-3)] - \frac{1}{280h}[\psi(4)-\psi(-4)] + \frac{h^8}{630}\psi^{(9)} \tag{24}$$

with $h = \Delta s = 1$. The simulation (see figures 12 and 13) shows that using the formula with order equal to 8, the estimation of the slope is extremely close to the theoretical value (the centroid of the triangular spot can be easily calculated and its value is equal to 11).

4.3.3 Problems linked to numerical calculations

For simulations with signals as Gaussian functions, we must be careful that we work with samples of continuous functions. So a theoretically symmetrical function won't be symmetrical anymore if we consider it in our simulations. For example, figures 14 and 15 show 16 samples of a Gaussian function. It is obvious that this signal is not symmetrical: so it is normal to have distortions on the phase. We can notice that theses distorsions are important in the high frequencies; as we are mostly interested in the DC frequency for the FPS method, it will not be a real problem. If we really want to get rid of this problem, we can use a threshold and discard all signal values beneath it, to recover a symmetrical function. In real simulations, our signals will be asymmetrical because of noise and other distorsions, so the point mentioned above is completely academic.

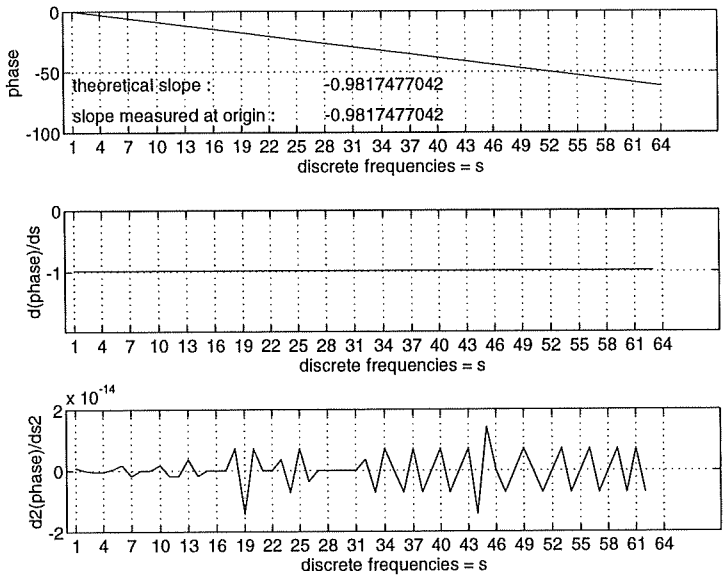

Figure 11: Phase, first derivative of phase and second derivative: the phase is effectively a straight line

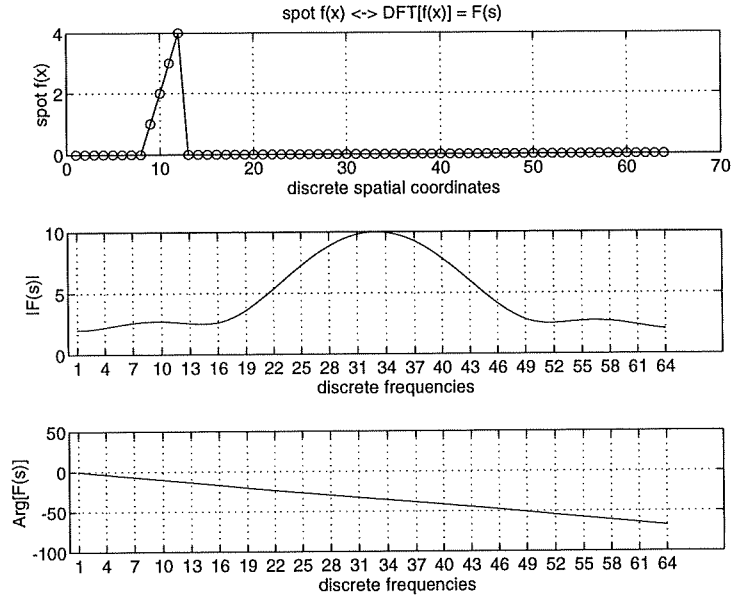

Figure 12: Triangular signal, modulus of its Fourier transform and phase

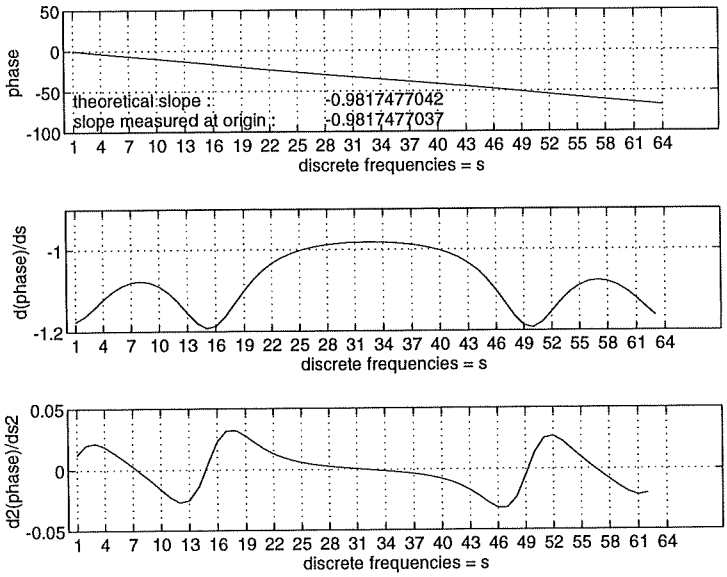

Figure 13: Phase, first derivative of phase and second derivative: the phase is not a perfect straight line as shown by its first derivative

We must notice that for the method to be used properly, we must work with signals sampled at frequency satisfying the Nyquist criterion. A discussion on it can be found in [9].

We also must point out that the phase calculated by FFT is defined modulo 2π and that we must take care of unwraping problems. A "hand-made" code has been writen for this purpose: it is extremely important to have a correct unwraping algorithm if we want to apply our method.

In addition, it appears (after simulations) that the evaluation of the slope (21) is better at order 2 than at order 8.

4.3.4 Measurement of the asymmetry of a function - Coefficient of skewness

Theoretically, the spot measured by the sensor array must be represented by an Airy function, which can be approximated by a Gaussian function. As we are interested in studying the effect of asymmetry on FPS method, we need a means to describe how much asymmetrical is a function. This problem has been solved in statistics, and mathematicians refer as skewness, the departure of a frequency distribution from symmetry. A quite complete description of skewness can be found in [28].

Suppose we have a frequency function $f(x)$ (or probability density). For a symmetrical distribution, mean, median and mode [4] coincide.

It is natural to take the deviation mean to mode or mean to median as measuring the skewness of the distribution. So, K. Pearson proposed the coefficient $Sk = \frac{mean-mode}{standarddeviation}$ to describe the skewness. Other coefficients exist (see [27]), but they involve calculation of the distribution median. We can point out that it is neither straightforward to calculate the mode of $f(x)$. Fortunately, it can be shown that [27] "for a large class of curves to which the moderately skew humped curve is a close approximation", the skewness of the formula above is exactly given by:

$$Sk = \frac{\sqrt{\beta_1}.(\beta_2 + 3)}{2[5\beta_2 - 6\beta_1 - 9]} \tag{25}$$

[4] The mode (or modal value) of the frequency function $f(x)$ is the solution of the equation $\begin{cases} \dot{f}(x) = 0 \\ \ddot{f}(x) < 0 \end{cases}$; the solution of $\begin{cases} \dot{f}(x) = 0 \\ \ddot{f}(x) > 0 \end{cases}$ is called antimode

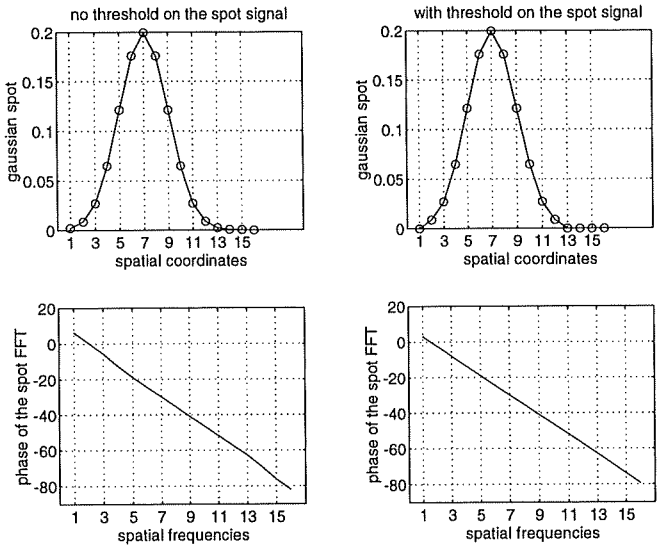

Figure 14: Gaussian shape with the phase of its FFT (on left) and Gaussian shape truncated beneath a threshold with the phase of its FFT (on right)

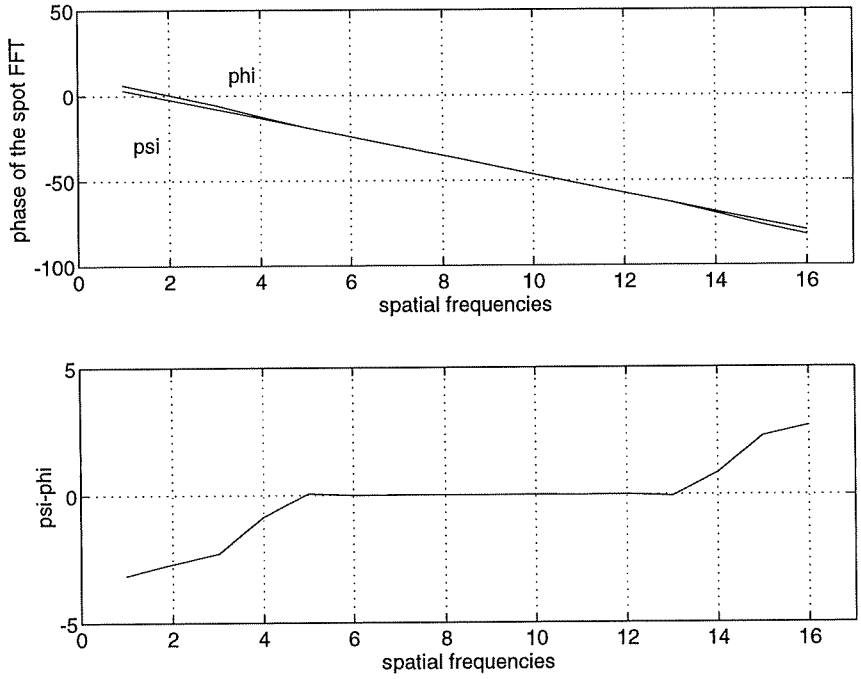

Figure 15: Comparison of the phases of the two signals of figure above

where $\beta_1 = \frac{\mu_3^2}{\mu_2^3}$, $\beta_2 = \frac{\mu_4}{\mu_2^2}$ and μ_1, μ_2, μ_3, μ_4,the first four moments of $f(x)$.

The drawback of this definition is that Sk is not limited, but this is a slight drawback (for moderately skew single-humped curves, it is usually less than unity). As we work with numerical signals, we have used the definition below to calculate the moments:

$$\mu_n = \frac{\sum_k f_k.k^n}{\sum_k f_k} \tag{26}$$

where $f_k = f(k)$ is the sample value of $f(x)$ in $x = k$. To study the effect of asymmetry on FPS method, we will generate a 1D distorted Gaussian, displaced from the origin of a distance x_o (imposed and known). We will evaluate x_o with FPS method (we will call x_{om} the measured value) and study the dependance of the relative error $e = \frac{x_o - x_{om}}{x_o}$ with the skewness Sk.

4.3.5 Simulations with strong distorted signals

We will call $f(x)$ the ideal Gaussian function and $h(x)$ the distorted Gaussian function. As $f(x)$ is symmetrical, it can be expressed by a series of even power

$$f(x) = \sum_n a_{2n} x^{2n}$$

If we consider the function $g(x) = tanh(\alpha x) + 1$, we can write that

$$g(x) = \sum_n b_{2n+1} x^{2n+1}$$

So by multiplying $f(x)$ with $g(x)$, we define the function $h(x)$ which holds both even power and odd power. We can notice that from an over point of view, the reference [26] shows that it is possible to analyse a skewed Gaussian shape with the Gram-Charlier expansion:

$$h(x) = g(x)\left[1 + \sum_{n=1}^{N} \frac{c_n}{n!} H_n(x)\right]$$

Coefficients $\{c_n\}$ measure the departure from the pure Gaussian $g(x)$ and $\{H_n(x)\}$ are Hermite polynomials. Figure 16 shows differents distorted functions.

Once we have generated a distorted function, we must take care that the centroid of $h(x)$ is different from the centroid of $f(x)$. So if we want to compare x_o (linked to $f(x)$) and x_{om} (linked to $h(x)$), we must recenter $h(x)$ on x_o. That means we need to calculate the centroid x_h of $h(x)$, and to use the function $h[x + x_h - x_o]$ for the FPS method. The centroid x_h is simply the first moment μ_1 of $h(x)$.

In figure 17 different asymmetrical Gaussian functions are displayed, and the skewness of each curve has been reported on the bottom graph. The equation of asymmetrical Gaussian functions is given by:

$$f(x) = \{tanh\,[coef * (x - 33)] + 1\} * \frac{1}{\sqrt{2\pi}.10}.e^{-\frac{(x-33)^2}{2.10^2}} \tag{27}$$

The variable "coef" is used to generate different asymmetrical Gaussian functions. For each, the skewness has been calculated with the formula 25.

To evaluate the ability of FPS algorithm to find the displacement of asymmetrical signals, we have generated distorted Gaussian profiles defined by 16 sampled only (in the further 2D simulations we will work on a sensor array of 16*16 pixels). The ideal spot (symmetrical Gaussian profile) is located in $x = 8$ (fixed). So the slope of the phase that we must theoreticaly find should be $-2\pi\frac{8}{16} = -\pi$. This value is reported on the figure 18 below. We have used the method described above to distort the profile. For each profile the skewness has been calculated and the slope of the phase measured. The results are ploted in figure

18. We see that the errors between measurements and the ideal value are very important. In fact as explained above, when we distort the profile, the centroid displaces.

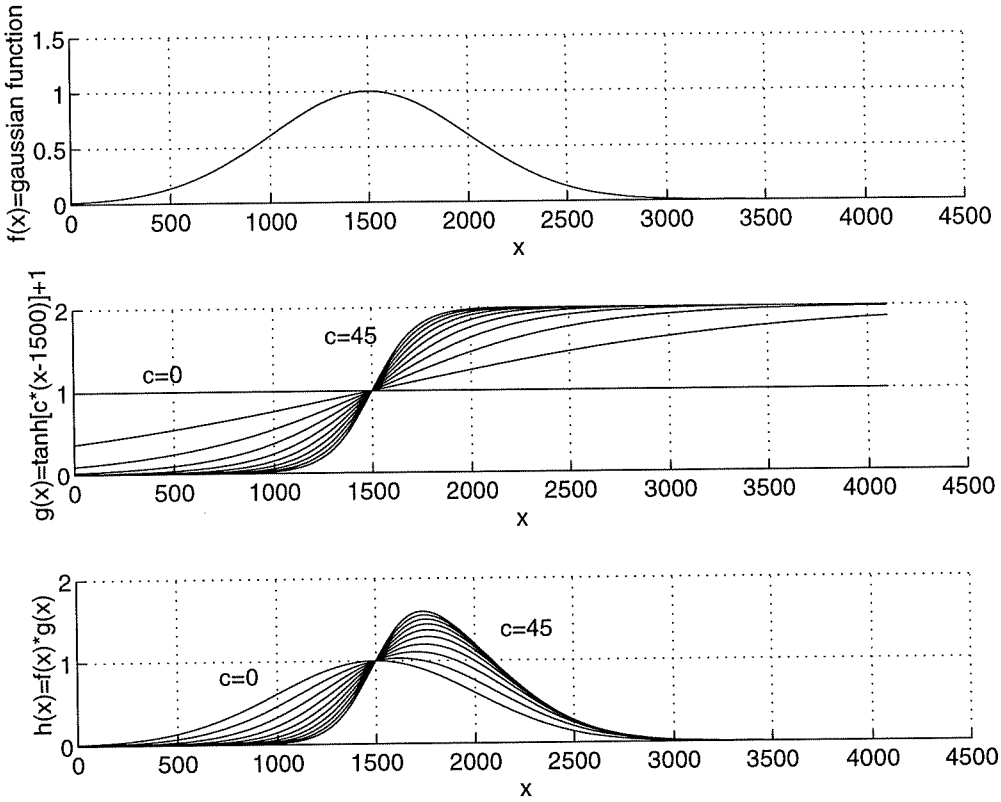

Figure 16: Generation of strong distorted Gaussian profiles

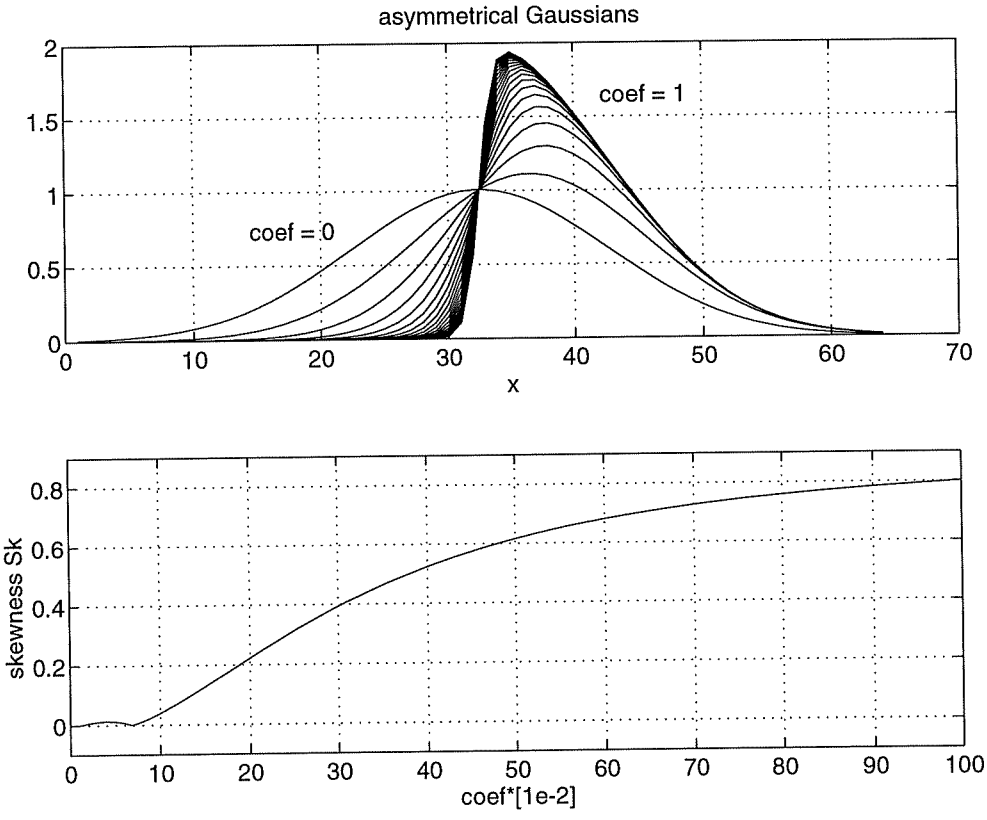

Figure 17: Asymmetrical Gaussians (top) and corresponding skewness (bottom)

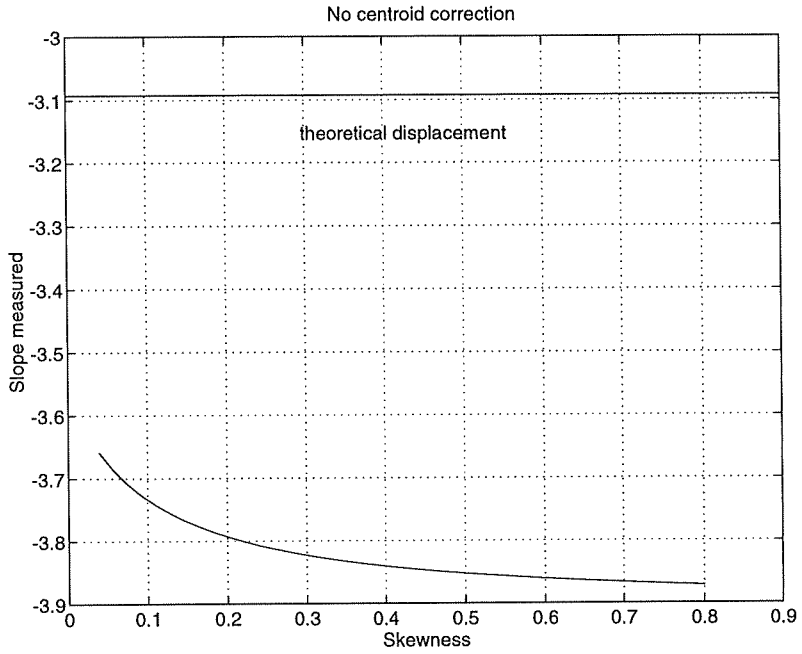

Figure 18: When the ideal Gaussian shape is distorted, the centroid is displaced, and the error measured becomes important

This is why we have calculated the centroid (with equation 6) of each distorted profile. So, for each asymmetrical Gaussian profile, the slope of the phase and the centroid have been ploted (figure 19). We see that there is a linear dependance between the slope of the phase (of the Fourier transform of the asymmetrical function measured at the DC frequency) and the centroid value. In other words, the relation found in 20 is correct.

4.4 Generalized FPS method for 2D spots

In this section we will explain how to generalize the method seen in 4.2, to two-dimensional signals.

We will consider a two-dimensional function $f(x, y)$, non-necessarily symmetrical, supposed describing the spot "centred" (see 4.2). We will call $g(x, y)$ the spot displaced of (x_o, y_o) from the origin 0, because of the plane wave tilt, with $g(x, y) = f(x - x_o, y - y_o)$. We have so $G(u, v) = F(u, v)e^{-2\pi i(ux_o + vy_o)}$, with $F(u, v) = \mathcal{F}[f(x, y)] = R(u, v) + iI(u, v)$ To simplify the notations, we pose $\theta = ux_o + vy_o$ and we define the modulus and the phase of $G(u, v)$ in the usual way:

$$G(u, v) = |G(u, v)|e^{iArg[G(u,v)]} = |G(u, v)|e^{i\psi(u,v)} \tag{28}$$

As in 4.2, we will call $a(u, v)$ the expression above:

$$a(u, v) = tan[\psi(u, v)] = \frac{Im[G(s)]}{Re[G(s)]} \tag{29}$$

As $G(u, v) = [R(u, v) + iI(u, v)].[cos(2\pi\theta) - isin(2\pi\theta)]$, we have simply :

$$a(u, v) = \frac{I(u, v)cos(2\pi\theta) - R(u, v)sin(2\pi\theta)}{R(u, v)cos(2\pi\theta) + I(u, v)sin(2\pi\theta)} \tag{30}$$

We can calculate the first partial derivative of $a(u, v)$ with u and we find:

$$\frac{\partial a(u, v)}{\partial u} = \frac{-2\pi x_o[I^2(u, v) + R^2(u, v)] + \frac{\partial I(u,v)}{\partial u}R(u, v) - \frac{\partial R(u,v)}{\partial u}I(u, v)}{[R(u, v)cos(2\pi\theta) + I(u, v)sin(2\pi\theta)]^2} \tag{31}$$

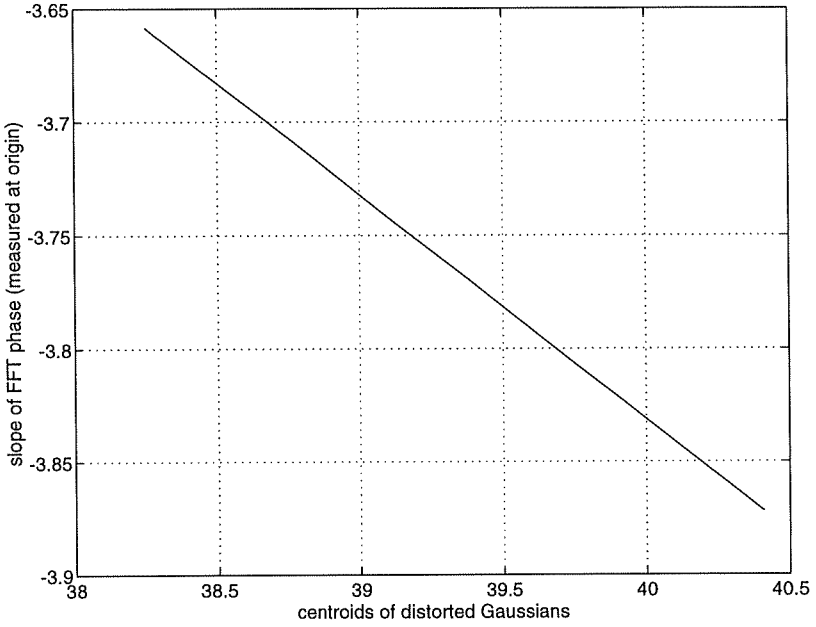

Figure 19: The FPS algorithm return the centroid value of a spot of any shape

As in 4.2, we want to evaluate $\frac{\partial a(u,v)}{\partial u}$ in $u = v = 0$. The problem is to get rid of the expression $\frac{\partial I(u,v)}{\partial u}R(u,v) - \frac{\partial R(u,v)}{\partial u}I(u,v)$ in $u = v = 0$. This problem could be avoided in 4.2 because it was possible to express any function as the sum of an even and an odd function, and to find the relations 16. This can not be generalized straightforward in two dimensions. Fortunately, we can use results given in [24] for example, to write:

$$\frac{1}{F(u,v)}.\frac{\partial F(u,v)}{\partial u}\Big)_{u=v=0} = -2\pi i < f >_x \tag{32}$$

where $< f >_x$ is the centroid of the function $f(x,y)$ in the x direction. As $F(u,v) = R(u,v) + iI(u,v)$, we have $\frac{\partial F}{\partial u} = \frac{\partial R}{\partial u} + i\frac{\partial I}{\partial u}$ and we can calculate:

$$\frac{1}{F(u,v)}.\frac{\partial F(u,v)}{\partial u}\Big)_{u=v=0} = \frac{\left(\frac{\partial R}{u}.R + \frac{\partial I}{u}.I\right) + i\left(\frac{\partial I}{u}.R - \frac{\partial R}{u}.I\right)}{R^2 + I^2}\Bigg)_{u=v=0} = -2\pi i < f >_x \tag{33}$$

where $< f >_x$ is necessarily real. So we have:

$$\frac{\partial R}{\partial u}.R + \frac{\partial I}{\partial u}.I\Big)_{u=v=0} = 0 \tag{34}$$

and

$$\frac{\frac{\partial I}{\partial u}.R - \frac{\partial R}{\partial u}.I}{R^2 + I^2}\Bigg)_{u=v=0} = -2\pi i < f >_x \tag{35}$$

By replacing 35 in 31, we have:

$$\frac{\partial a(u,v)}{\partial u} = \left[\frac{I^2(0) + R^2(0)}{R^2(0)}\right](-2\pi)\left[x_o + < f >_x\right] \tag{36}$$

But we know that:

$$F(u,v) = \int_{-\infty}^{\infty}\int_{-\infty}^{\infty} f(x,y)e^{-2\pi i(ux+vy)dxdy} = R(u,v) + iI(u,v) \tag{37}$$

thus,

$$F(0,0) = \int_{-\infty}^{\infty}\int_{-\infty}^{\infty} f(x,y)dxdy = R(0,0) + iI(0,0) \tag{38}$$

As $f(x,y)$ is real, we have $I(0,0) = 0$ and finally:

$$\frac{\partial a(u,v)}{\partial u}\Big)_{u=v=0} = (-2\pi)\left[x_o + < f >_x\right] \tag{39}$$

As we have defined $a(u,v)$ as $a(u,v) = tan\left[\psi(u,v)\right]$, we get $\frac{\partial a(u,v)}{\partial u} = \frac{\partial \psi(u,v)}{\partial u}.\frac{1}{cos^2[\psi(u,v)]}$ and finally:

$$\frac{\partial \psi(u,v)}{\partial u}\Big)_{u=v=0} = -2\pi\left[x_o + < f >_x\right].cos^2[\psi(0,0)] \tag{40}$$

$$\frac{\partial \psi(u,v)}{\partial v}\Big)_{u=v=0} = -2\pi\left[y_o + < f >_y\right].cos^2[\psi(0,0)] \tag{41}$$

We can notice that if $g(x,y)$ is real, then $G(0,0) = \int_{-\infty}^{\infty}\int_{-\infty}^{\infty} g(x,y)dxdy$ is real, so $\frac{\partial a(u,v)}{\partial u}\Big)_{u=v=0} = \frac{Im[G(0,0)]}{Re[G(0,0)]} = 0$ and $tan[\psi(0,0)] = a(0,0) = 0$ imply that $\psi(0,0) = n\pi$ with $n \in \mathcal{Z}$. Thus it is clear that $cos^2[\psi(0,0)] = 1$. In addition, $< f >_x$ and $< f >_y$ are by definition, the centroids of the spot centred $f(x,y)$. They must be equal to zero, if $x = y = 0$ is the origin of axis. To conclude, we can say that:

$$\frac{\partial \psi(u,v)}{\partial u}\Big)_{u=v=0} = -2\pi x_o \tag{42}$$

$$\frac{\partial \psi(u,v)}{\partial v}\Big)_{u=v=0} = -2\pi y_o \tag{43}$$

with

$$\psi(u,v) = Arg\left\{\mathcal{F}\left[g(x,y)\right]\right\} \tag{44}$$

4.5 Simulations with 2D spots

The aim of these simulations is to study the importance of errors due to the algorithm itself, and those due to the noise.

4.5.1 The spot signals generated

As explained in 3.2.5 it is possible to assume that the spot to study is a Gaussian shape instead of an Airy disk. This has been done in this work. We have decided to consider a sensor array of 16 by 16 pixels. All the displacements will be expressed in unity of pixels. The analytical expression of a two-dimensional Gaussian profile is given by:

$$f(x,y) = \frac{1}{\sqrt{2\pi\sigma^2}} e^{-\frac{(x-x_o)^2+(y-y_o)^2}{2\sigma^2}} \tag{45}$$

The figure 20 displays the Gaussian spots generated for different values of σ.

The figure 21 below summarize the generation of a quantized and noisy Gaussian shape. The threshold (used to get a symmetrical signal), has been fixed to $1/20th$ of the spot maximum. The noise added, as it will be explained further, is an additive noise with a uniform distribution [5]. We have assumed that the signal was quantized with 2^{16} levels (16 bits). In fact, with the sensor array chosen, the quantization does no seem to be of critical importance.

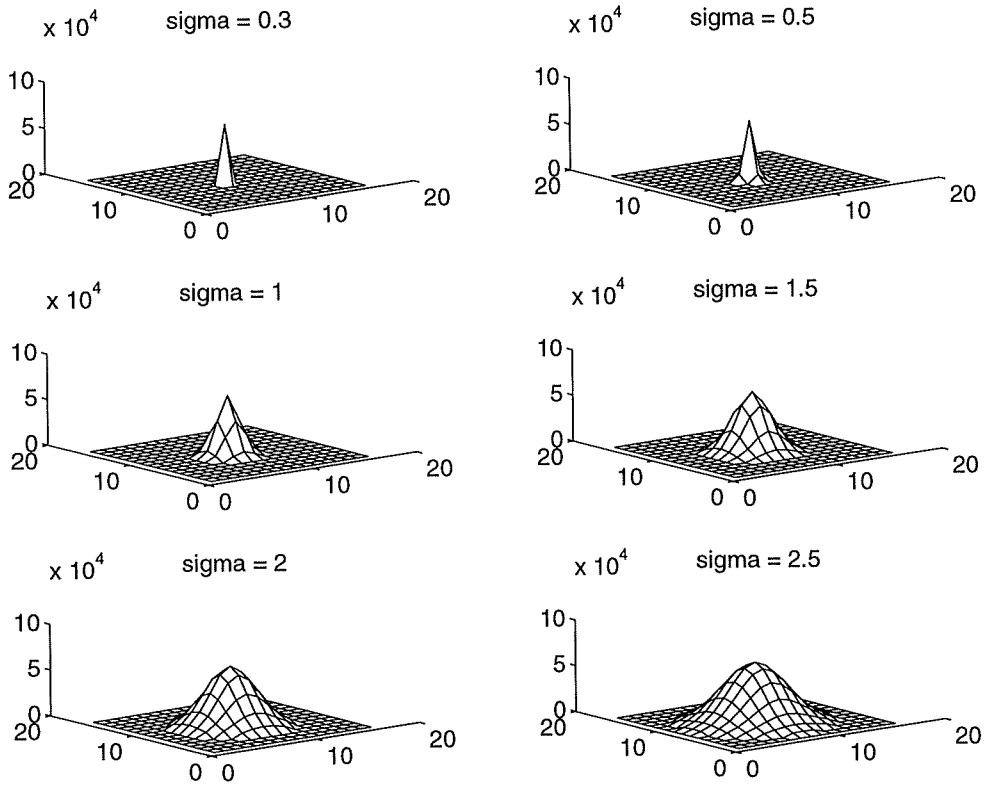

Figure 20:

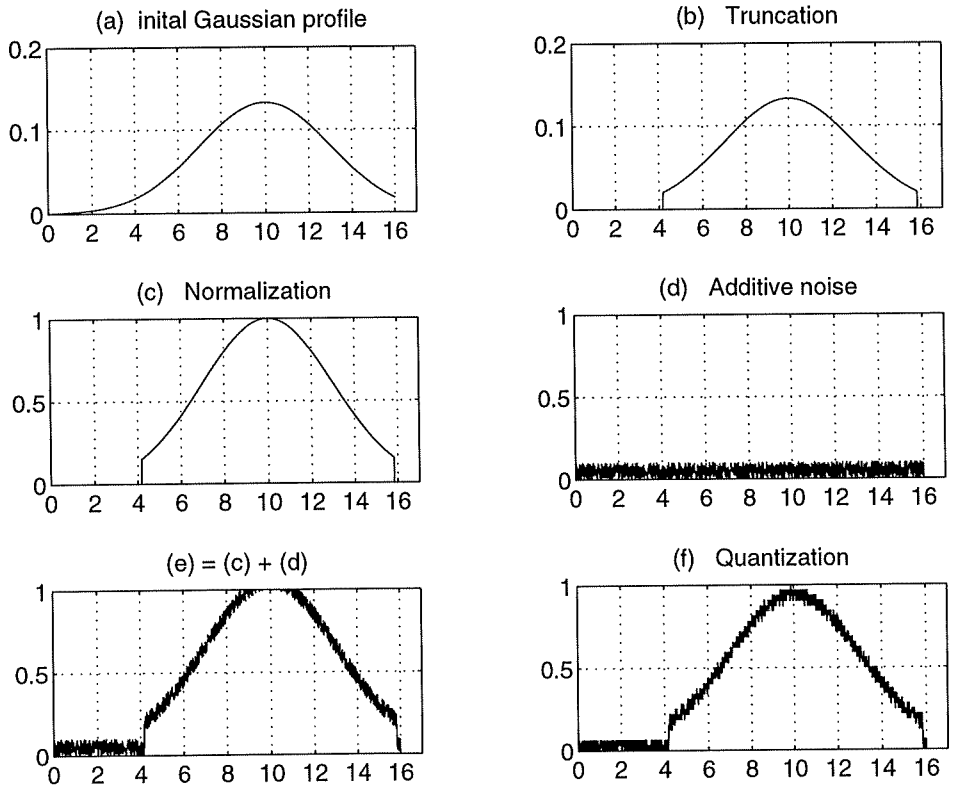

Figure 21:

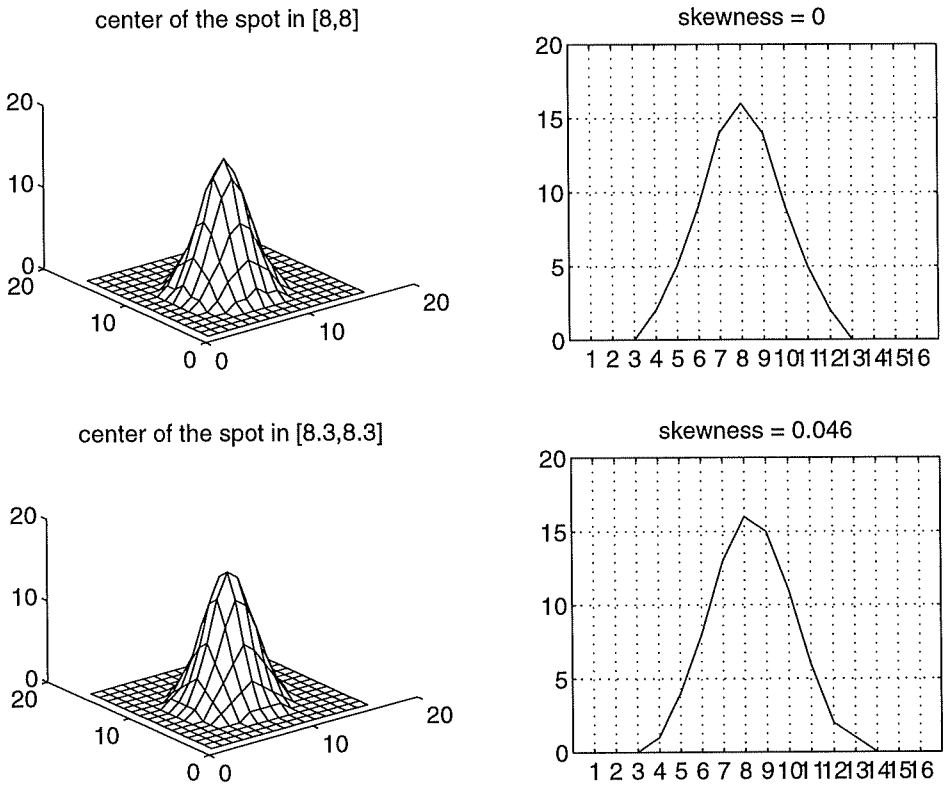

Figure 22: Effect of sampling on the symmetry of the spot

4.5.2 Errors due to algorithm

In their simulations, Fillard and al. [10] have found error of 1.5% pixels for "symmetrical" spots without noise. In fact, there is an error because the spot we assume to be symmetrical is not. The figure 22 shows what happens in one dimension.

The skewness is 0 when the spot is precisely located on a pixel, and significantly different from zero when it is not the case. This phenomenon is the source of errors found when there is no noise on the spot considered. We will call this type of error, "sampling error". An other type of error occures when the spot is truncated: this happens when the size of the spot is too important compared to the size of array. We will call this type of error, "truncation error". Figure 23 gives an example.

We have done some simulations with a Gaussian spot located at the pixel $(8, 8)$. The error between coordinates found by the generalized FPS method and the ideal coordinates, has been found to be of 10^{-13} pixel.

To evaluate the sampling error, we have decided to move the spot in the domain $\mathcal{D}$ showed at figure 24. We have generated 50*50 ideal spots, and for each spot, we have apply our algorithm, that has given us the measured location of the spot. Because of symmetry, we have only taken care of the x coordinates. In the figure 25, the 50*50 errors between x_o (ideal location of the spots) and x_m (measured location of the spots), have been ploted for $\sigma = 0.5$ and $\sigma = 2$. We can see that the error is about 5% for the first plot, and 2% for the second one. These values are of the same order than those found by Fillard ([10]).

To have an idea of the error, we have calculated the mean and the standard deviation of the 50*50 error coefficients. The figure 26 shows the results found.

The formula used are these ones:

[5] We must point out that concerning the noise added, figure 21 is not realistic. The noise is of course only added at the 16*16 pixels locations.

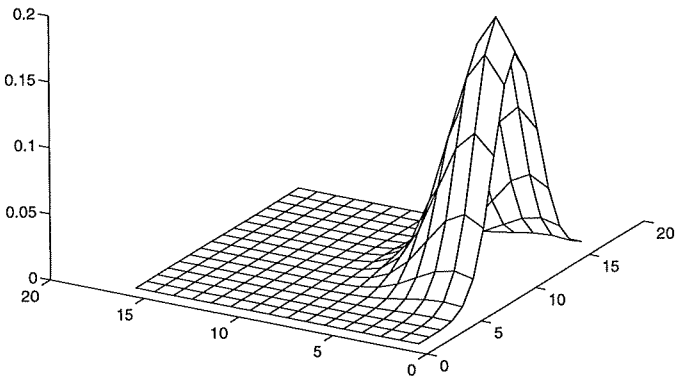

Figure 23:

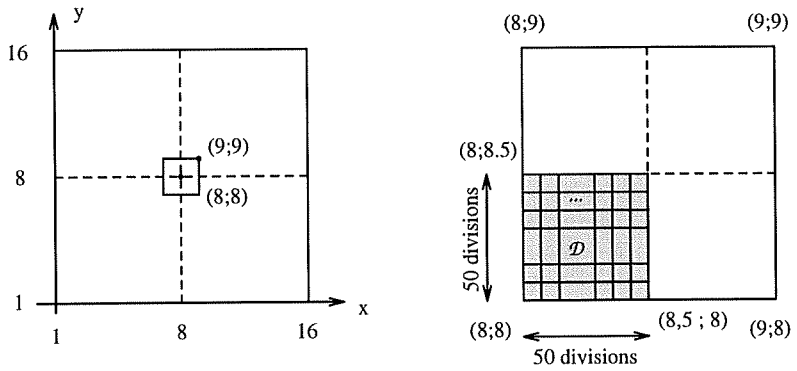

Figure 24:

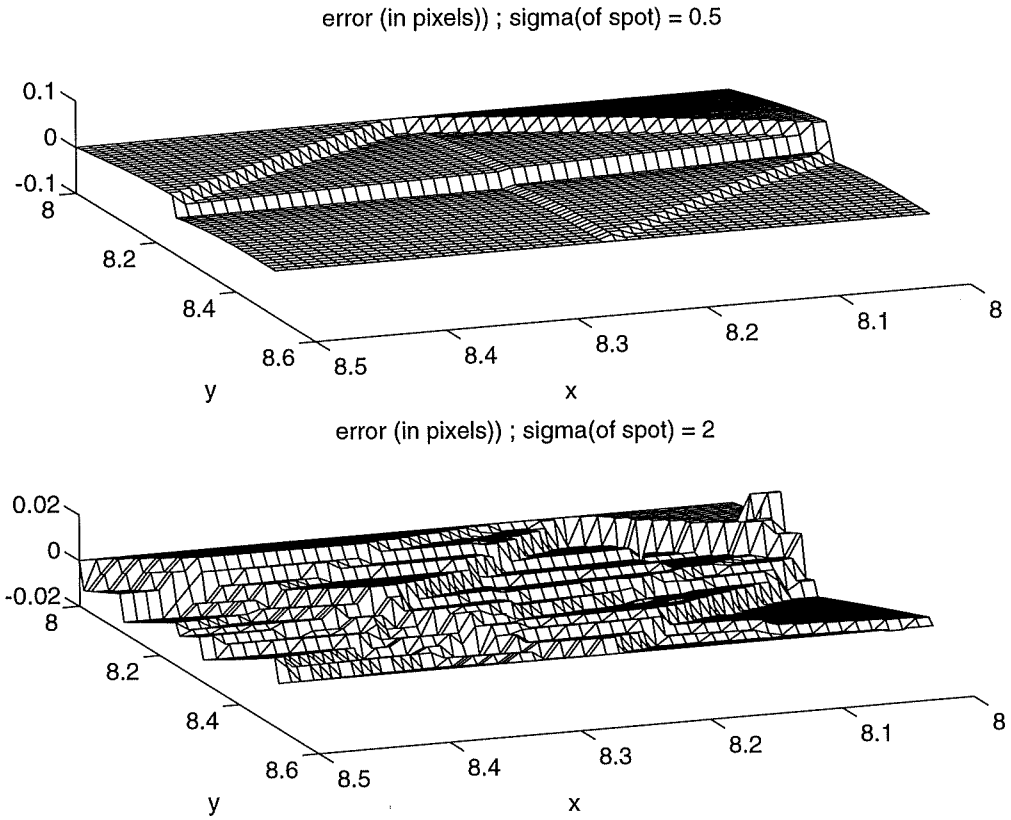

Figure 25:

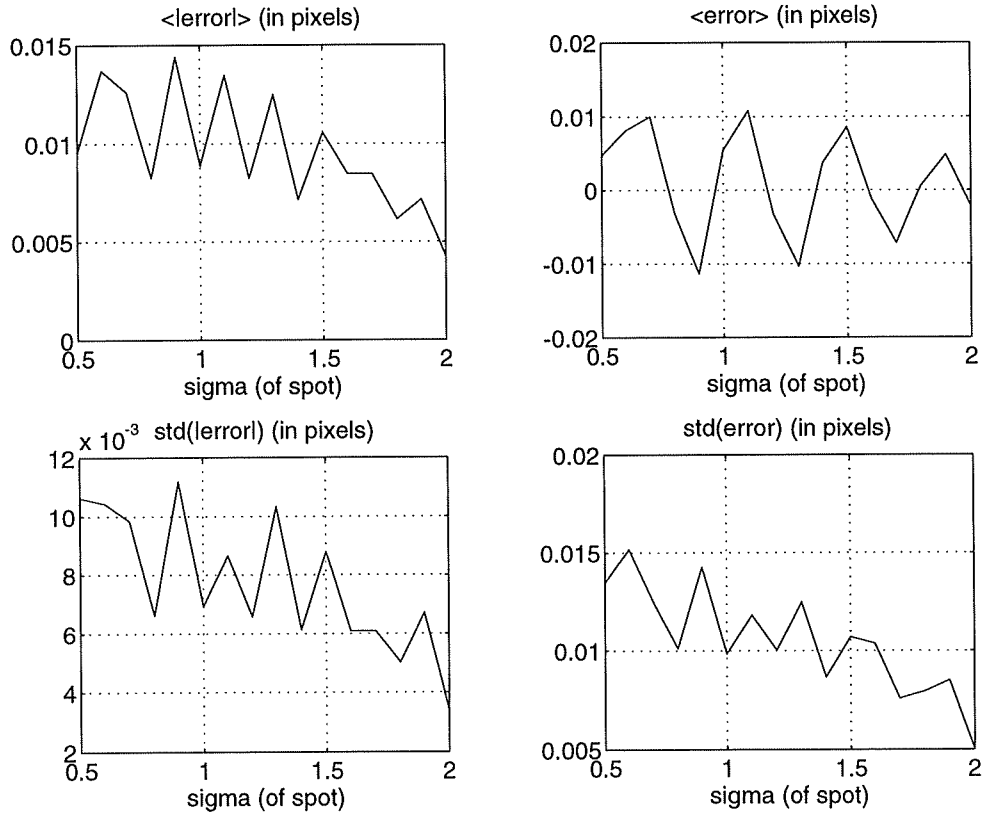

Figure 26:

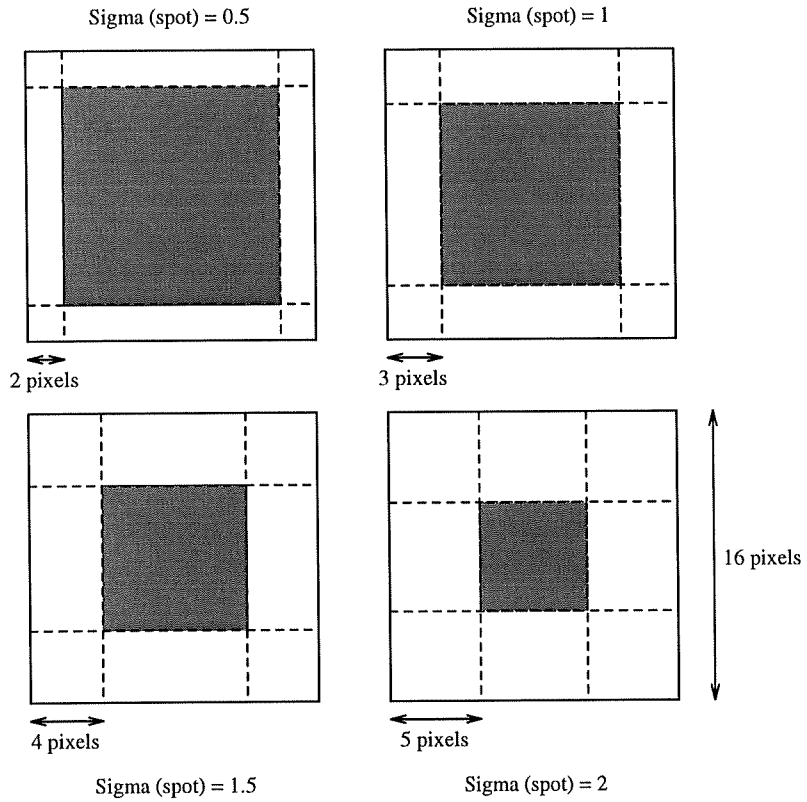

Figure 27:

$$< error >= \frac{1}{N} \sum_{x_o} \sum_{y_o} e_x(x_o, y_o) \tag{46}$$

$$std(error) = Var^{\frac{1}{2}}(e_x) \tag{47}$$

$$< |error| >= \frac{1}{N} \sum_{x_o} \sum_{y_o} |e_x(x_o, y_o)| \tag{48}$$

$$std(|error|) = Var^{\frac{1}{2}}(|e_x|) \tag{49}$$

with (x_o, y_o) in the domain $\mathcal{D}$, $N = 50 * 50$ and $e_x(x_o, y_o) = x_o - x_m$.

Conclusions:

The standard deviation decreases when the spot sigma (width spot) increases. So ideally, to minimize the error, we should maximize the sigma of the spot. But we must take care that in this simulation, the spot is centred in $(8, 8)$ (the center of sensor array). As a matter of fact we will encounter problem of truncation error if the sigma becomes too large. After simulations, we have found that no truncations errors were encountered when the spot was located in the areas displayed in figure 27 below.

It is clear that if we minimize the sampling error, we will reduce the area of the sensor array in which the spot is allowed to be without truncation errors. We can also point out that if the spot sigma is too big, we will encounter problems linked to Nyquist criterion. So a trade-off is to be found.

4.5.3 Errors due to the noise

In this section, we will present a study of noise effects on the algorithm accuracy. To only study the effect of noise, we must not have sampling and truncation errors. This is why, we have located the spot in the center of sensor array, so in $(8, 8)$. When there is no noise, the error found between the measured coordinates and the ideal coordinates is about 10^{-13} pixels. For reasons of simplicity, we have decided

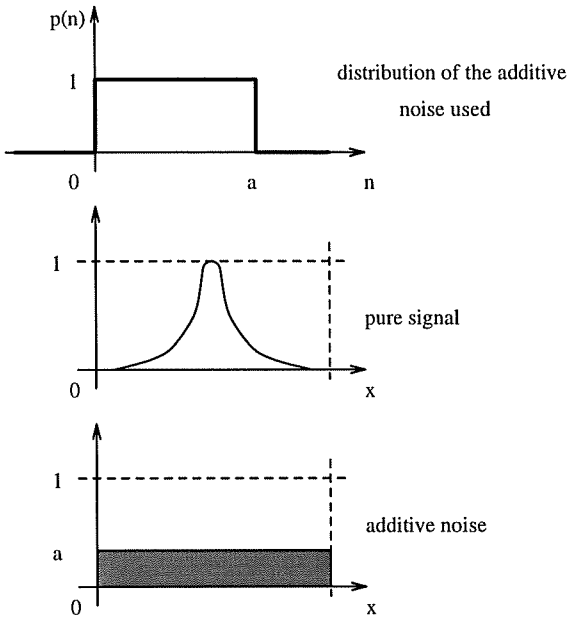

Figure 28:

to add to our ideal (and perfectly symmetrical) spot, an additive noise, with a uniform distribution, [6]as it is shown in figure 28.

To quantify the noise, we have used the definition of SNR below:

$$SNR = \frac{mean\ of\ pure\ signal}{standard\ deviation\ of\ noise} \tag{50}$$

In our simulations we have also used the ratio " a" equal to the amplitude of noise (=a) divided by the maximum of the signal (=1). The drawback of this coefficient is that it does not take into account the width of the spot. With the type of noise used, we can calculate the SNR with the formula:

$$SNR = \frac{\frac{1}{16*16}\sum_{i=1}^{16}\sum_{j=1}^{16} f(i,j)}{\frac{a}{\sqrt{(12)}}} \tag{51}$$

Figure 29 displays noisy Gaussian spots with a SNR fixed to 1, and figure 30 displays noisy Gaussian spots with a coefficient "a" fixed to 0.2. The "sigma" displayed in the figure titles corresponds to the sigma (width) of the spots.

We have fixed the ideal spot (without noise) at position $(x_o, y_o) = (8, 8)$. For a given spot sigma and a given characteristic of noise (either the SNR or the coefficient "a"), we have generated 1000 noisy Gaussian spots and measured the corresponding centroids (x_m, y_m). Figure 31 displays the 1000 errors values $x_o - x_m$ for two given characteristics of noise.

We can see that error seems to be unbiaised and that the standard deviation seems to increase linearly with the coefficient "a". To verify this, we have calculated the means and standard deviations of errors, for coefficients "a" between 0 and 0.1. The results are given in figure 32 below.

To have an idea of the SNR values corresponding to the coefficient "a", we can say that:

- sigma(spot) = 0.5 : $a = 0.1$ corresponds to $SNR = 0.209$
- sigma(spot) = 1 : $a = 0.1$ corresponds to $SNR = 0.825$
- sigma(spot) = 1.5 : $a = 0.1$ corresponds to $SNR = 1.837$

[6]It is clear that this type of noise is not realistic but it was a first step in our study. Unfortunately, we have not had time enough to study other types of noise.

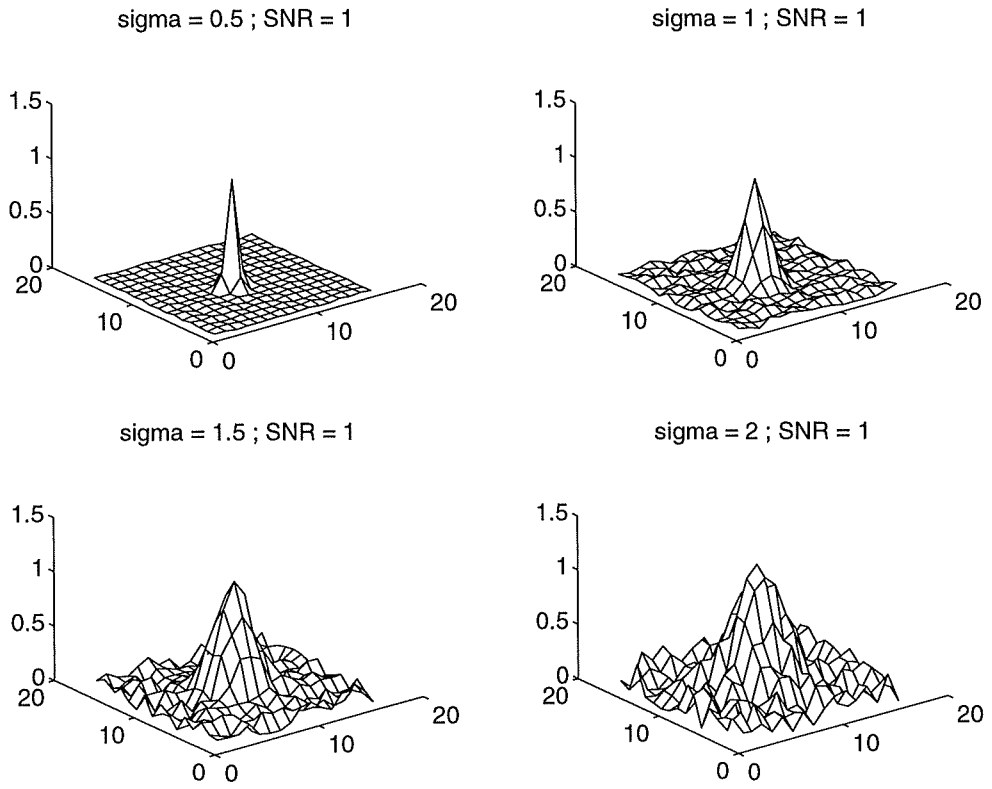

Figure 29:

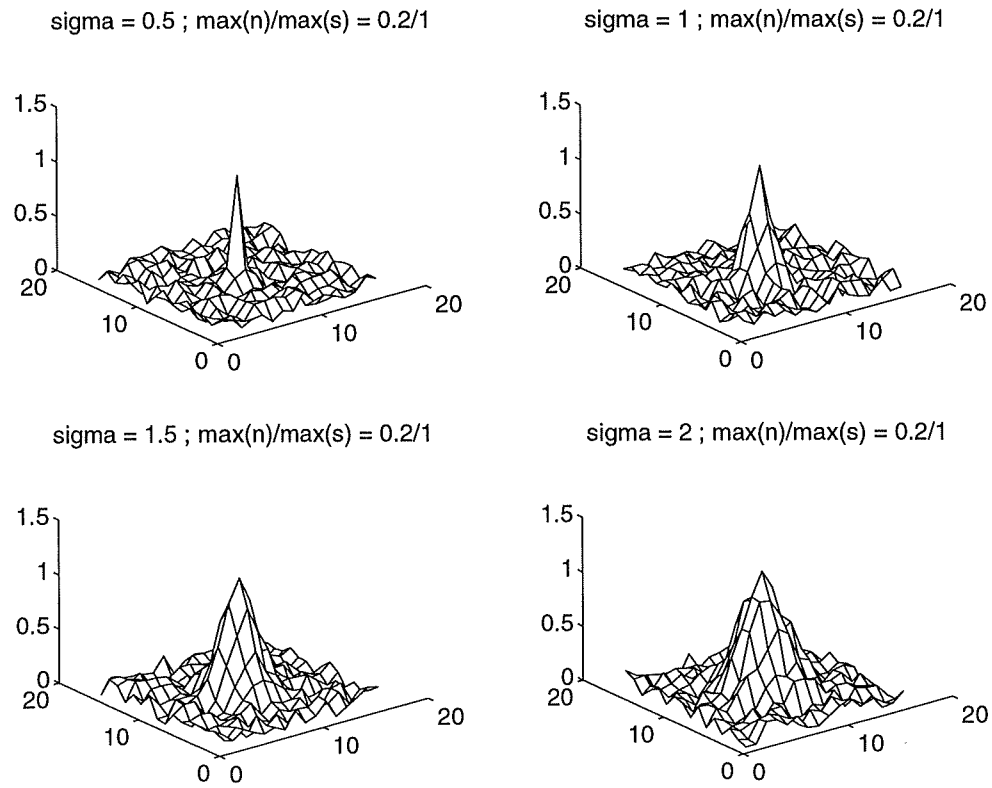

Figure 30:

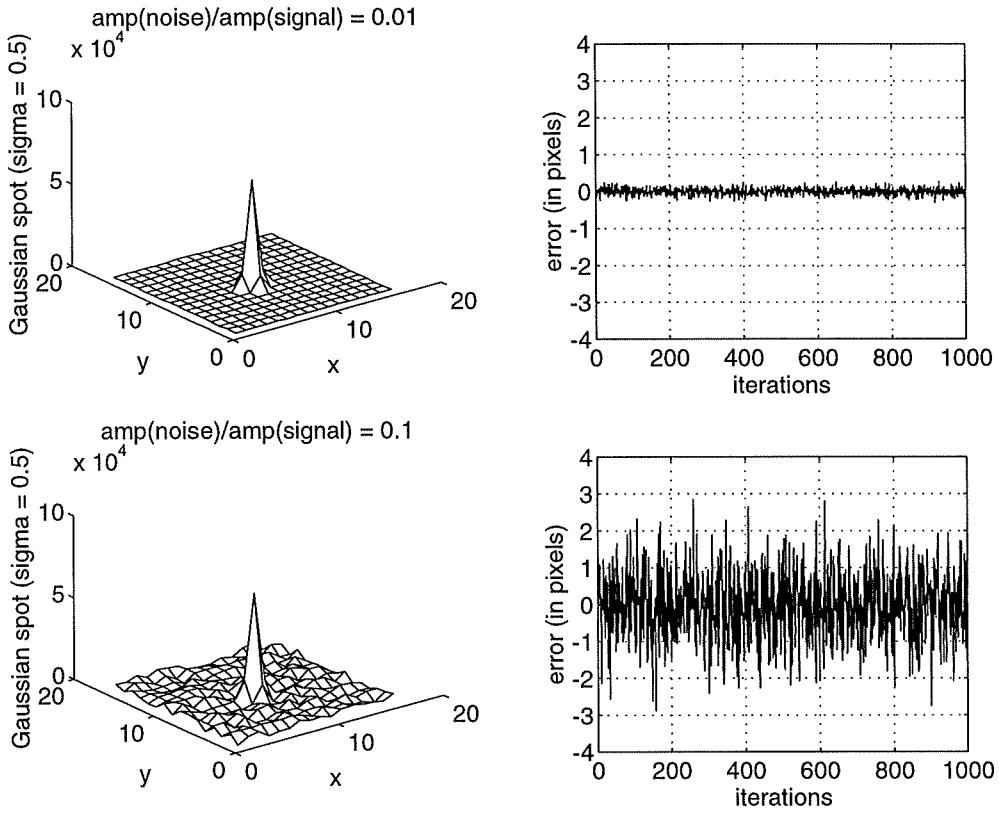

Figure 31:

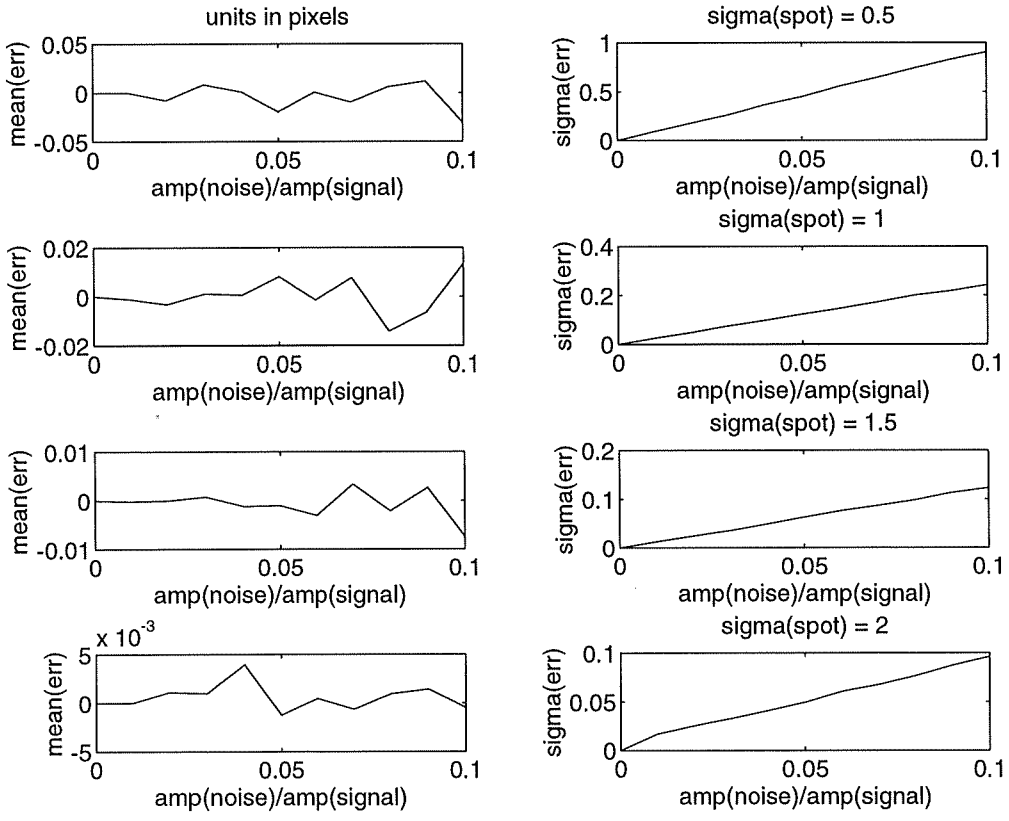

Figure 32:

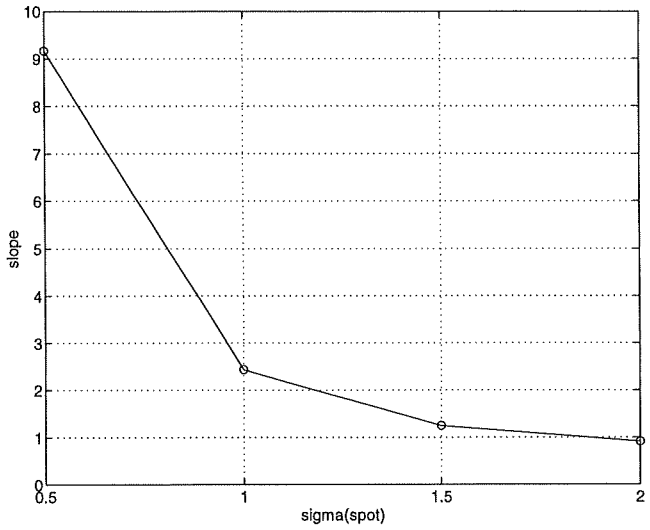

Figure 33:

- sigma(spot) = 2 : $a = 0.1$ corresponds to $SNR = 3.189$
- for all sigma(spot), $a = 0$ corresponds to $SNR = \infty$

We observe that there is actually a linear relation between the noise standard deviation and the coefficient "a". A linear regression has been done (least mean square fit) and the slopes of the lines have been ploted in figure 33 for the four spot sigma.

But we must take care that a coefficient "a" of 0.1 for a spot signal of 0.5 will give a different SNR than those calculated with a coefficient "a" of 0.1 for a spot signal of 2. This is why we have plotted the standard deviation of errors according to the SNR. The result is given in figure 34. We observe an exponential law that seems to be independant of the spot width.

Conclusions:

For the type of noise studied, we observe that there is a linear relation between the error standard deviation and the noise coefficient "a". We have shown it is equivalent to say that there is a exponential relation between the error standard deviation and the SNR. An interesting thing is that this law does not depend on the spot width.

5 Conclusion

The aim of this work was to study the effect of asymmetry on the FPS method proposed by Fillard [9] [10]. This has been done and we have shown it was possible to generalize this method to functions of any shapes, provided that the phase would be evaluated at the DC frequency only. We have encountered a lot of problems especially linked to the phase unwraping. A study of noise on the generalized method has been made with an additive noise uniformly distributed. Unfortunately, we have not had time to study other more realistic types of noises. The original aim of this work was to compare FSP method with Imperial College method, but by lack of time, this could not have been done. To conclude, it appears that the larger is the spot (spot sigma), and the less is the sampling error, but we must not forget that if the spot is too large, we will encounter problem linked to truncation and Nyquist criterion. The sampling error is about 1.5% pixels for spot with a sigma of 0.5 and can be of 0.5% pixels for spot with a sigma of 2. The error due to the noise has been found to follow an exponential law independant of the spot width.

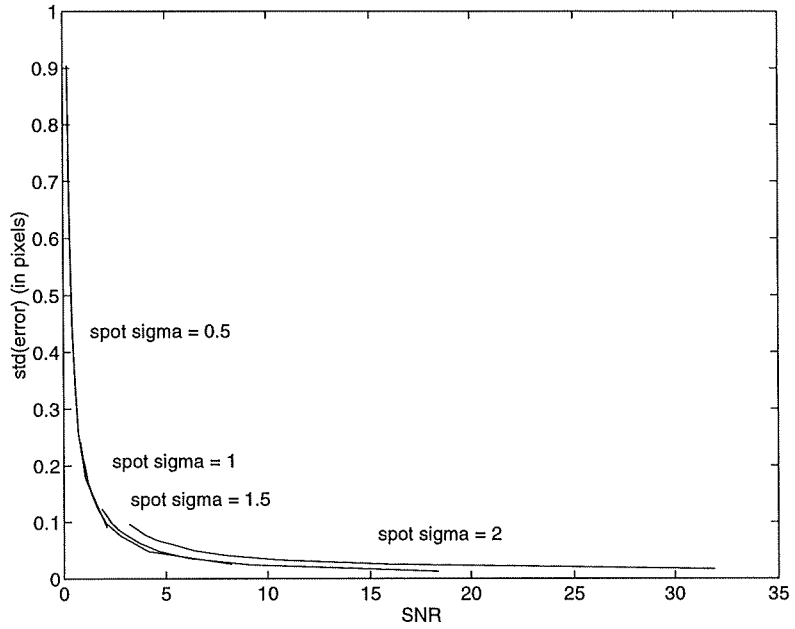

Figure 34:

References

[1] B. F. Alexander and N. C. Ng. *Elimination of systematic error in sub-pixel accuracy centroid estimation Opt. Engineering 30, 1320, 1991*

[2] K. Cameron *ACE Automatic centroid extractor for real time target tracking Northcon conference, Record 1990 00133-138*

[3] Genrui Cao and Xin Yu *Accuracy analysis of a Hartmann-Shack wavefront sensor operated with a faint object Opt. Engineering 33, 2331, 1994*

[4] J. A. Cox *Evaluation of peak location algorithms with subpixel accuracy for mosaic focal planes Proc. SPIE 292, 288, 1981*

[5] E. W. Dennison and R. H. Stanton *Ultra-precise star tracking using CCDs SPIE. Proc. 252, 54, 1980*

[6] D. Down *Image-position error associated with a focal plane array J. Opt. Soc. Am. (A) 9, 700, 1992*

[7] M. Elbaum and P. Diament *Estimation of image centroid, size, and orientation with laser radar Appl. Opt. 16, 2433, 1977*

[8] M. Elbaum, N. Orenstein and J. MacEachin *Algorithms for estimating image position SPIE Proc. 252, 98, 1980*

[9] J. P. Fillard *Subpixel accuracy location estimation from digital signals Opt. Engineering 31, 2465, 1992*

[10] J. P. Fillard, H. M'timet, J. M. Lussert and M. Castagne *Computer simulation of super-resolution point source image detection Opt. Engineering 32, 2936, 1993*

[11] S. B. Grossman and R. B. Emmons *Performance analysis and size optimisation of focal planes for point source tracking algorithm applications Opt. Engineering 23, 167, 1984*

[12] E. P. Lyvers, O. R. Mitchell, M. L. Akey and A. P. Reeves *Subpixel measurements using a moment based edge operator IEEE. Trans. PAMI 11, 1293, 1989*

[13] H. J. Meyer et al. *Fast centroiding with a 24*24 frame transfer CCD Proc. SPIE 1900, 91, 1993*

[14] J. S. Morgan, D. C. Slater, J. G. Timothy and E. B. Jenkins *Centroid position measurements and subpixel sensitivity variations with the MAMA detector Appl. Opt. 28, 1178, 1989*

[15] J. Nowakowski and M. Elbaum *Fundamental limits in estimating light pattern position J. Opt. Soc. Am. 73, 1744, 1983*

[16] P. M. Salomon and T. A. Glavich *Image signal processing in sub-pixel accuracy star trackers SPIE Proc. 252, 64, 1980*

[17] P. Seitz *Optical super-resolution using solid state cameras and digital processing Opt. Engineering 27, 535, 1988*

[18] R. S. Stobie *Application of moments to the analysis of panoramic atronomical photographs SPIE Proc. 264, 208, 1980*

[19] D. W. Tyler, G. Rousset, S. R. Restaino and G. C. Loos *Low light-level adaptive optics for a two-telescope interferometer sheme - includes a simulated comparison of a cross-correlation S-H slope algorithm with a conventional intensity-centroid Proc. SPIE 2029, 380, 1993*

[20] K. A. Winick *Cramer-Rao lower bounds on the performance of CCD optical position estimators J. Opt. Soc. Am. (A) 3, 1809, 1986*

[21] Zhi-Yong and Zhen-Kang Shen *A new filtering method for precision target tracking Proc. SPIE National Aerospace and Electronics Conference (NAECON) 1,369, 1992*

[22] J. S. Boland, H. S. Ranganath, W. W. Malcom *Computational efficiency of multiple image registration algorithms SPIE Vol. 252 Smart Sensors II (1980), 105, 1980*

[23] S. R. Restaino, R. W. Conley, G. C. Loos, R. R. Radick *Image deconvolution from pupil masking experiment SPIE Vol. 2029 Digital image recovery and synthesis II 1993, 390-399*

[24] R. M. Bracewell *The Fourier Transform and its Applications Mc GrawHill, New York, 1965*

[25] B. E. A. Saleh, M. C. Teich *Fondamentals of Photonics, John Wiley&Sons, New York, 1991*

[26] B. R. Frieden *Probability, Statistical Optics, and Data Testing, Springer-Verlag, Berlin, 1983*

[27] G. U. Yule, M. G. Kendall *An Introduction to the Theory of Statistics, Charles Griffin&Company Limited, London, 1950*

[28] M. G. Kendall *The Advanced Theory of Statistics, Charles Griffin&Company Limited, London, 1948*

[29] W. E. Milne *Numerical Calculus, Princetown University Press, Princetown, 1949*

[30] R. K. Tyson *Principles of Adaptive Optics, Academic Press, Boston, 1991*